Available online at www.sciencedirect.com
ScienceDirect
Chemical Geology 250 (2008) 49–67
CHEMICAL GEOLOGY INCLUDING ISOTOPE GEOSCIENCE
www.elsevier.com/locate/chemgeo

Contribution of syncollisional felsic magmatism to continental crust growth: A case study of the Paleogene Linzizong volcanic Succession in southern Tibet

Xuanxue Mo [a], Yaoling Niu [b,*], Guochen Dong [a], Zhidan Zhao [a], Zengqian Hou [c], Su Zhou [a], Shan Ke [a]

[a] State Key Laboratory of Geological Processes and Mineral Resources, School of Earth Science and Mineral Resources, China University of Geosciences, Beijing, 100083, China
[b] Department of Earth Sciences, Durham University, Durham DH1 3LE, UK
[c] Institute of Geology, Chinese Academy of Geological Sciences, Beijing 100037, China

Received 9 July 2007; received in revised form 26 January 2008; accepted 4 February 2008

Editor: R.L. Rudnick

Abstract

The Linzizong volcanic succession (~65–45 Ma) and the coeval batholiths (~60−40 Ma) of andesitic to rhyolitic composition represent a magmatic response to the India–Asia continental collision that began at ~70–65 Ma and ended at ~45–40 Ma with convergence continuing to present. These syncollisional felsic magmatic rocks are widely distributed along much of the >1500 km long Gangdese Belt immediately north of the India–Asia suture (Yarlung–Zangbo) in southern Tibet. Our study of the Linzizong volcanic rocks from the Linzhou Basin (near Lhasa) suggests that syncollisional felsic magmatism may in fact account for much of the *net* contribution to continental crust growth. These volcanic rocks show a first-order temporal change from the andesitic lower Dianzhong Formation (64.4–60.6 Ma), to the dacitic middle Nianbo Formation (~54 Ma), and to the rhyolitic upper Pana Formation (48.7–43.9 Ma). The three formations show no systematic but overlapping Nd–Sr isotope variations. The isotopically depleted samples with $\varepsilon_{Nd(t)}>0$ indicate that their primary sources are of mantle origin. The best source candidate in the broad context of Tethyan ocean closing and India–Asia collision is the remaining part of the Tethyan ocean crust. This ocean crust melts when reaching its hydrous solidus during and soon after the collision in the amphibolite facies, producing andesitic melts parental to the Linzizong volcanic succession (and the coeval batholiths) with inherited mantle isotopic signatures. Ilmenite as a residual phase (plus the effect of residual amphibole) of amphibolite melting accounts for the depletion of Nb, Ta and Ti in the melt. The effect of ocean crust alteration plus involvement of mature crustal materials (e.g., recycled terrigeneous sediments) enhances the abundances of Ba, Rb, Th, U, K and Pb in the melt, thus giving the rocks an "arc-like" geochemical signature. Residual amphibole that possesses super-chondritic Nb/Ta ratio explains the sub-chondritic Nb/Ta ratio in the melt; residual plagioclase explains the slightly depleted, not enriched, Sr (and Eu) in the melt, typical of continental crust. These observations and reasoning plus the remarkable compositional similarity between the andesitic lower Dianzhong Formation and the model bulk continental crust corroborates our proposal that continental collision zones may be sites of net crustal growth (juvenile crust) through process of syncollisional felsic magmatism. While these interpretations are reasonable in terms of straightforward petrology, geochemistry and tectonics, they require further testing.

Keywords: Continental collision; Net crustal growth; Tibetan Plateau; Linzizong volcanic succession

1. Introduction

The continental crust comprises no more than ~0.5% of the Earth's mass, but it is an important geochemical reservoir because it is enriched in many incompatible elements, and contains more than ~30% of Earth's Ba, Rb, Th, U, K, Pb budget (Taylor and McLennan, 1995; Rudnick, 1995; Rudnick

* Corresponding author.
E-mail address: Yaoling.Niu@durham.ac.uk (Y. Niu).

0009-2541/$ - see front matter © 2008 Elsevier B.V. All rights reserved.
doi:10.1016/j.chemgeo.2008.02.003

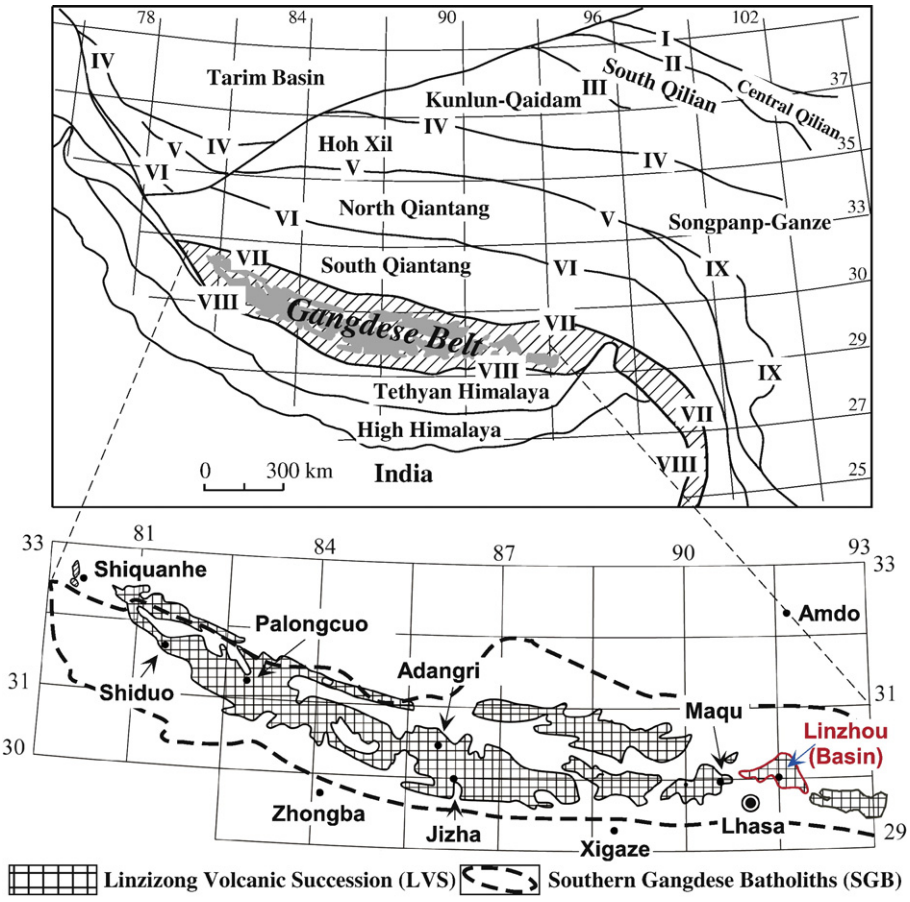

Fig. 1. Top: the Tibetan plateau comprises a number of accreted blocks separated by suture zones indicated with thick lines and Roman numerals. The >1200 km long Linzizong Volcanic Succession (LVS) (grey patches) in the >1500 km long Gangdese Belt (stippled area) between Bangong–Nujiang (VII) and Yarlung–Zangbo (VIII) sutures are highlighted. Bottom: close-up of the LVS and the spatial distribution of the Southern Gangdese Batholiths (SGB) simplified from the 1:250,000 scale geologic map (Pan et al., 2004). Detailed mapping and stratigraphy (Dong, 2002) of the LVS were carried out in the Linzhou Basin as indicated. Modified from Mo et al. (2003) and Zhou et al. (2004).

and Fountain, 1995; McDonough and Sun, 1995; Rudnick and Gao, 2003). While bulk composition of continental crust is reasonably well established (Rudnick and Gao, 2003), a genuine understanding of its origin, mode and rate of accretion, and how it has acquired its "andesite" bulk composition from mantle derived materials remains speculative (e.g, Rudnick and Gao, 2003; Kelemen et al., 2003a,b; Plank, 2005; Davidson and Arculus, 2006). The broad similarity in trace element geochemistry between bulk continental crust and island arc volcanic rocks (i.e., the "arc-like signature", characterized by depletion of Nb, Ta, Ti etc. relative to enrichment of Ba, Rb, U, K, Pb etc.) suggests a genetic link (Taylor and McLennan, 1985), which led to the "andesite" or "island arc" model for the origin of continental crust (Taylor, 1967, 1977). Geochemical calculations suggest that at least 80% of the crustal mass was generated by subduction-zone magmatism (Plank and Langmuir, 1998; Barth et al., 2000). On the other hand, recognition of model age "spikes" (e.g., McCulloch and Bennett, 1994; Condie, 2000) preserved in the geologic record suggests that pulses of mantle derived melts, perhaps in the form of "mantle plumes" (e.g., oceanic plateaus and continental flood basalts), must also have contributed episodically to the crustal mass (Stein and Hofmann, 1994; Abbott and Mooney, 1995; Abbott et al., 1997; Polat et al., 1998; Albarède, 1998; Condie, 2000; Niu et al., 2003; Kerr, 2003; Kemp et al., 2006; Hawkesworth and Kemp, 2006).

If we assume that continental crust is ultimately derived from mantle melts, both at island arc settings and from intraplate environments, then any successful model for continental crust growth must be able to address two obvious questions: (1) what physical mechanisms may have effectively transformed the dominantly mafic mantle derived materials into the andesitic continental crust composition, and (2) what processes may have amassed intra-ocean island arcs and "scattered" oceanic plateaus to join the existing continents. There has been much effort to address the first question in the context of subduction-zone magmatism because primitive arc melts and bulk arc crust are too mafic (e.g., Gill, 1981; Arculus, 1981; Pearcy et al., 1990). Removal of mafic/ultramafic lower arc crust cumulate beneath active arc or during orogenesis is a popular idea (e.g., Kay and Kay, 1993; Rudnick, 1995; Plank, 2005) to explain why only felsic arc lithologies contribute to continental crust, although physical mechanisms for such removal may be complex (Jull and Kelemen, 2001).

Slab melting and melt-mantle interactions are thought to be an important mechanism to produce high magnesian andesites

(HMA vs. basaltic melts) resembling continental crust composition (Kelemen, 1995; Kelemen et al., 2003b; Tatsumi, 2006). However, this requires not only warm slabs but also unusually hot mantle wedge that is rare at present (Tatsumi, 2006), and modern bulk arc crust is mafic anyway. Likewise, adakites (Defant and Drummond, 1990) are a variation of HMA with "garnet-signature" resembling the more abundant TTG suite produced in the Archean when the mantle was hotter. Present-day adakites, once thought to be unique product of slab melting, can in fact be formed in different tectonic settings by various means (see Castillo, 2006).

Nevertheless, continental crustal materials may indeed be forming at present along island arcs such as the Izu–Bonin–Mariana arc system (e.g., Takahashi et al., 2007), but it is unclear how intra-oceanic arcs contribute to continental growth because they are moving away from continents; back arc basins spread and ocean basins spread also. Importantly, it has been demonstrated quantitatively that crustal addition by subduction-zone magmatism is mass balanced by crustal loss through sediment subduction and subduction erosion (von Huene and Scholl, 1991; Scholl and von Huene, 2004; Clift and Vannucchi, 2004) on modern Earth. Furthermore, isotopic studies demand that crustal recycling at subduction zones has been important since ~2.0 Ga (Kramers and Tolstikhin, 1997). Therefore, active subduction zones may not be sites for net continental growth.

In this paper, we use the geochemistry of the Linzizong Volcanic Succession (LVS), which is compositionally andesitic to rhyolitic, in southern Tibet (Fig. 1) to hypothesize that partial melting of the remaining part of the Tethyan ocean crust, or the leading edge of the Indian plate, during and shortly after India–Asia collision may be responsible for these felsic volcanic rocks and the coeval South Gangdese batholiths (SGB). The Linzizong andesite, the basal section of the LVS with mantle isotopic signature, resembles remarkably the model bulk composition of continental crust (Rudnick and Gao, 2003) in terms of abundances of most elements and key elemental ratios. If our hypothesis for the syncollisional felsic magmatism is proved to be of general significance, then continental collision zones are ideal sites of crustal growth, which relieves the need of some unknown process or processes to return the more mafic component of the arc crust to the mantle required by the "island arc" model. We stress that our hypothesis does not answer the question when and how the first continental crust formed, but offers alternatives to explain "juvenile" crust formation and continental crust growth with fewer difficulties.

2. Paleogene Linzizong volcanic succession in southern Tibet

The Linzizong Volcanic Succession (LVS, andesitic to rhyolitic in composition) of the Gangdese Belt in southern Tibet (Fig. 1) offers a prime opportunity to test our hypothesis highlighted in the previous section. The LVS rocks (1) are syncollisional, emplaced during the India–Asia collision from a "soft" touch at ~70–65 Ma to a "hard" clash at ~45–40 Ma (e.g., Yin and Harrison, 2000; Flower et al., 2001; Mo et al., 2002, 2003, 2006, 2007), thus representing the material witness of the continental collision process with time; (2) they are volcanic rocks (vs. crystalline intrusives), and thus have recorded more faithfully signals of magma generation and evolution; (3) they distribute extensively along much of the Gangdese Belt for ~1200 km (Fig. 1) with well defined/documented stratigraphy in the Linzhou basin, thus allowing detailed examination of how the volcanism may have changed in time in response to the collision; (4) they are likely co-genetic with the giant South Gangdese Batholiths (SGB; Fig. 1), thus allowing proper evaluation of total juvenile crustal mass; (5) they also contain much younger (25–10 Ma) ultrahigh-potassic lavas, allowing the study of their petrogenesis in the context of the collision and aftermath; and importantly (6) the Himalaya is the world's youngest and still active orogenic belt today, hence, the result of this work may serve as a reference for studying collision-associated magmatism and crustal formation in the geologic record.

2.1. Regional geology

The Tibetan Plateau is a geological amalgamation as a result of several continental collision events since the Early Paleozoic (e.g., Allègre et al., 1984; Dewey et al., 1988; Yin and Harrison, 2000) (Fig. 1). The Gangdese Belt, also called Lhasa Terrane, is the southernmost Eurasian block immediately north of the Yarlung–Zangbo suture (VIII in Fig. 1) of the India–Asia collision. The Gangdese Belt is considered as an Andean-type active continental margin prior to the collision beginning ~70–65 Ma (Yin and Harrison, 2000; Flower et al., 2001; Mo et al., 2003, 2006, 2007), and is interpreted as rifted from Gondwana (Leeder et al., 1988; Pearce and Mei, 1988) before it collided with Eurasia along the Bangong–Nujiang suture (VII in Fig. 1). The basement of the Gangdese Belt is poorly exposed, but may consist largely of the Cambrian Amdo gneisses (Harris et al., 1986; Dewey et al., 1988) and perhaps also of older and more complex lithologies (e.g., Yin and Harrison, 2000; Kapp et al., 2003). While shallow marine sequences of Paleozoic and Mesozoic crop out in many localities (metamorphosed to slates, phyllites, schists, gneisses, amphibolites and migmatites) (Leeder et al., 1988; Yin et al., 1988; Willems et al., 1996; Murphy et al., 1997; Yin et al., 1999; Kapp et al., 2003), the Gangdese Belt contains numerous granitoid batholiths (hence the name Trans-Himalayan Batholiths). They are older in the north (>150 Ma), and younger towards the south (e.g, Yin and Harrison, 2000). The South Gangdese Batholiths (SGB) belt is dominated by 60–40 Ma composite plutons (Scharer et al., 1984; Copeland et al., 1987; Jiang et al., 1999; Mo et al., 2005), extends E–W for up to 2000 km, and accounts for ~45% of all the batholiths exposed in the Gangdese Belt. The SGB intrusives share time and space with the LVS (Mo et al., 2005; Dong et al., 2005), but were previously interpreted as resulting from Tethyan seafloor subduction beneath the Eurasian Andean-type continental margin (Allègre et al., 1984; Dewey et al., 1988; Pearce and Mei, 1988) based on the then accepted view that the India–Asia collision commenced at ~45 Ma. The older batholiths to the north are interpreted as resulting from southward subduction of the

Table 1
Simplified stratigraphy of the Linzizong Volcanic Succession in Linzhou Basin, southern Tibet

Time period		Formation	Thickness	^{40}Ar–^{39}Ar age	Description
Quaternary loose sediments: fluvial sands, gravels, boulders, collapses, and loess etc.					
Tertiary	Neogene	Pana	>2000	48.73 to 43.9 Ma	Mainly high potassic (high-K) rhyolitic ignimbrites with inter-layered alluvial sedimentary rocks
		Nianbo	~720	~54 Ma	Mostly rhyolitic, dacitic and basaltic trachy-andesitic rocks intercalated with beds of lacustrine limestones and tuffs
	Paleogene	Dianzhong	~2300	64.4 to 60.6 Ma	Mostly andesitic lavas (~50%) and pyroclastic deposits (~50%) with increasing trachy-andesite and dacite upwards
Angular unconformity on top the Cretaceous Shexing Group (K/T unconformity)					
Late Cretaceous		Shexing group			Strongly deformed sandstone, siltstone and slate

Qiangtang terrane (Fig. 1) (Pearce and Mei, 1988; Yin and Harrison, 2000; Kapp et al., 2003, 2005), but some juvenile crust materials have been recognized there recently using zircon Hf isotopes (Chu et al., 2006).

A prominent phenomenon in the Gangdese Belt is the strongly deformed Cretaceous strata that show conspicuous regional unconformity with the overlying undeformed LVS volcanic strata of subaerial eruption (Allègre et al., 1984; Coulon et al., 1986; Willems et al., 1996; Dong, 2002; Mo et al., 2003, 2006, 2007). Recent 1:250,000 scale geologic mapping of the Gangdese Belt (Pan et al., 2004) revealed that the LVS distributes extensively, extending E–W for >1200 km long and taking >50% outcrop area of the entire Gangdese Belt (Fig. 1). This unconformity goes with the LVS throughout the entire Gangdese Belt, suggesting a major tectonic event, which, together with the geochronological data (Zhou et al., 2004), allows Mo and co-authors (Dong, 2002; Mo et al., 2002, 2003; Zhou et al., 2004; Mo et al., 2006, 2007) to advocate that the unconformity, which is ≥65 Ma, represents the onset of the India–Asia collision, supporting the inference of ~70–65 Ma by Yin and Harrison (2000) based on a multitude of observations.

2.2. Brief stratigraphy of the Linzizong Volcanic Succession (LVS)

So far, a relatively detailed study of the LVS rocks is limited to the Linzhou Basin near Lhasa (Fig. 1) (Dong, 2002; Mo et al., 2003; Zhou et al., 2004), where the LVS has a total thickness of ~5000 m, readily subdivided into lower Dianzhong (LDF), middle Nianbo (MNF) and upper Pana (UPF) formations (Table 1) based on eruption hiatuses (Dong, 2002).

2.3. Ages of Linzizong volcanics

Previously reported ages for the LVS rocks vary in a narrow range of 49.2–56.2 Ma (Jin and Zhou, 1978; Maluski et al., 1982; Xu et al., 1985; Coulon et al., 1986), but the stratigraphic positions of the dated samples are unknown. Table 1 gives the best age dates on representative samples from the Linzhou Basin (Zhou et al., 2004), which place the LVS eruptions in the Paleocene to Early Eocene, suggesting a more-or-less continuous volcanic activity for ~20 Myrs. Recent 1:250,000 scale geologic mapping in the Gangdese Belt (Pan et al., 2004) has characterized the LVS in the entire Gangdese Belt and agreed in general with the stratigraphic column in the Linzhou Basin (Dong, 2002). However, some basal andesites of the LVS from Cuoqin in middle Gangdese and Ngari in western Gangdese gave whole-rock K–Ar ages of 58.6 Ma (Guogang Xie, pers. Comm., 2002) and 60.68 Ma (Guo et al., 1991), respectively. If these K–Ar dates are reliable, it would suggest somewhat diachronous onset of the LVS volcanism along the Gangdese Belt, while recognizing factors such as spatial variation of individual lava flows and sampling uncertainties in topographically complex terrenes.

3. Samples

A total of 17 samples (5 from each of the three formations and two mafic dykes) have been analyzed for major and trace elements. Three of these samples and an additional seven samples have been analyzed for Sr and Nd isotopes. These samples were collected in 2000 (except for sample L1108) as part of the project to establish the stratigraphic column of the LVS in the Linzhou Basin near Lhasa (Fig. 1) (see Dong, 2002). Rock types, sample locations and petrography of all these samples are summarized in Table 2. The geochemical data on these 24 samples and another 14 samples published previously (Mo et al., 2007) plus some unpublished (compositionally similar) data are used for discussion.

4. Analytical techniques

Bulk compositions were determined at the Key Laboratory of Continental Dynamics, Northwest University, China. Major elements were analyzed by XRF (Rikagu RIX 2100) using fused glass disks. Trace elements were analyzed by ICP-MS (Elan 6100 DRC) after total acid digestion in Teflon bombs and dilution. Some trace elements were also analyzed by XRF using powdered pellets. Concentrations of Sr, Y, Nb, Zr, Cr and Ni obtained by both methods agree well within 10%. Analyses of rock standards (AGV-1, GSR-01 and BCR-2)

Table 2
Petrography of studied samples from the Linzizong Volcanic Succession in Linzhou Basin, southern Tibet

Sample	Rock name	Formation	Longitude/latitude	Petrographic description
BD-77	Rhyolitic tuff	UPF	29°58.50′ N, 91°08.46′ E	Fresh; glass shards (>40%), crystal clasts of biotite, plagioclase and K-feldspar (~5% in total), rhyolite clasts (~15%) and very fine-grained volcanic ash (<40%); average clast size: <2 mm.
BD-103	Rhyolitic ignimbrite	UPF	30°00.64′ N, 91°08.42′ E	Massive and fresh; glass shards (~55%), crystal clasts of biotite, plagioclase, K-feldspar and quartz (~10% in total), rhyolite lasts (~35%); clast size: 2–6.5 mm.
BD-106	Rhyolitic ignimbrite	UPF	30°00.62′ N, 91°08.42′ E	Massive and fresh; glass shards (~65%), crystal clasts of biotite, plagioclase, quartz and K-feldspar (~10% in total), rhyolite clasts (~25%); average clast size: 2 mm.
BD-114	Rhyolitic tuff	UPF	30°02.25′ N, 91°08.43′ E	Fresh; glass shards (~80%), crystal clasts of biotite, plagioclase, quartz and K-feldspar (~10% in total), plastic rhyolitic clasts (~10%); average clast size: 2 mm.
LZ9916	Rhyolitic tuffaceous lava	UPF	30°00.52′ N,91°09.02′ E	Massive and fresh; glass shards (~78%), crystal clasts of plagioclase, quartz and K-feldspar (~10% in total), plastic rhyolitic clasts (~12%); average clast size: 2 mm.
LZ9917	Rhyolitic tuffaceous lava	UPF	30°00.52′ N, 91°09.02′ E,	Massive and fresh; glass shards (~75%), crystal clasts of biotite, plagioclase, quartz and K-feldspar (~10% in total), plastic rhyolitic clasts (~15%); average clast size: 2 mm.
P-1	Rhyolitic ignimbrite	UPF	29°59.18′ N, 91°09.00′ E	Massive and fresh; spherulitic; glass shards (~70%), crystal clasts of biotite and plagioclase (~10% in total), rhyolite clasts (~5%) and plastic rhyolitic clasts (~15%); average clast size: <2 mm.
BD-55	Welded rhyolitic tuff	MNF	29°58.73′ N, 91°10.28′ E	Fresh; glass shards (~45%), crystal clasts of plagioclase, biotite, quartz and K-feldspar (~10% in total), plastic rhyolitic clasts (~25%) and rhyolite clasts (~10%); average size of clasts; ~2 mm.
BD-65	Trachybasalt	MNF	29°59.05′ N, 91°10.20′ E	Porphyritic and fresh; ~35% phenocrysts and ~65% groundmass; phenocrysts: plagioclase (>20%), amphibole (>10%), and trace K-feldspar; K-feldspar in groundmass; average grain size: 2 mm for phenocrysts and 0.2 mm for groundmass.
LZ9910	Trachyandesite	MNF	29°57.89′ N, 91°07.52′ E	Porphyritic and fresh; ~30% phenocrysts and ~70% groundmass; phenocrysts: plagioclase (~15%), clinopyroxene (~10%) and magnetite (~5%); groundmass: plagioclase, magnetite and interstitial K-feldspar; average grain size: 2 mm for phenocrysts and 0.2 mm for groundmass.
LZ9921	Rhyolitic ignimbrite	MNF	29°58.85′ N, 91°11.15′ E	Massive and fresh; glass shards (~70%), crystal clasts of plagioclase, biotite, quartz and K-feldspar (~10% in total), plastic rhyolitic clasts (~20%); average size: 2 mm for clasts.
L060	Rhyolitic tuff	MNF	29°58.62′ N, 91°11.60′ E	Fresh; glass shards (~85%), crystal clasts of biotite, plagioclase, K-feldspar and quartz (~10% in total), rhyolite clasts (~5%); average size: 2 mm for clasts.
LZ994	Brecciaed rhyolitic tuff	MNF	29°57.89′ N, 91°07.52′ E	Fresh; glass shards (~70%), crystal clasts of biotite, plagioclase, K-feldspar and quartz (~10% in total), rhyolite clasts (~20%); clast size: 2–6 mm.
D-2	Trachyandesite	LDF	29°57.12′ N, 91°11.88′ E	Porphyritic; ~45% phenocrysts and ~55% groundmass; phenocrysts: plagioclase (~35%), amphibole (~5%) and K-feldspar (~5%); average grain size ~2 mm for phenocrysts and <0.2 mm for groundmass; overprinted with ~3 chlorite and ~3% calcite.
D-15	Andesite	LDF	29°57.85′ N, 91°11.33′ E	Porphyritic and fresh; ~45% phenocrysts and 55% groundmass;. Phenocrysts: plagioclase (~40%), amphibole (~5%); average grain size ~1.7 mm for phenocrysts and 0.2 mm for groundmass.
BD-27	Andesite	LDF	29°58.03′ N, 91°05.85′ E	Porphyritic and fresh; ~48% phenocrysts and ~52% groundmass; phenocrysts: plagioclase (~42%) and amphibole (~6%); average grain size 2 mm for phenocrysts and 0.2 mm for groundmass.
BD-123	Andesite	LDF	29°55.01′ N, 91°03.08′ E	Porphyritic and fresh; ~50% phenocrysts and ~50% groundmass; phenocrysts: plagioclase (~45%) and amphibole (~5%); average grain size: 3 mm for phenocrysts and 0.2 mm for groundmass.
BD-151	Andesite	LDF	29°58.05′ N, 91°12.46′ E	Porphyritic and fresh; ~45% phenocrysts and ~55% groundmass; phenocrysts: plagioclase (~40%) and amphibole (~5%); average grain size 2 mm for phenocrysts and 0.2 mm for groundmass.
BD-145	Andesite	LDF	29°57.19′ N, 91°11.92′ E	Porphyritic and fresh; ~35% phenocrysts and ~65% groundmass; phenocrysts: plagioclase (~30%), amphibole (~5%), and some quartz; groundmass: plagioclase microlites; average grain size: 3 mm for phenocrysts and for 0.3 mm for groundmass.
BD-160	Trachyandesite	LDF	29°58.35′ N, 91°10.56′ E	Porphyritic and fresh; ~45% phenocrysts and ~55% groundmass; phenocrysts: plagioclase (~40%) and amphibole (~5%); average grain size: 3 mm for phenocrysts and 0.3 mm for groundmass.
L-1108	Basaltic andesite	LDF	No GPS data (1993 sampling)	Porphyritic and fresh; ~40% phenocrysts and ~60% groundmass; phenocrysts: plagioclase (~30%), clinopyroxene (5%) and amphibole (~5%); average grain size: 2 mm for phenocrysts and 0.2 mm for groundmass.
BD-58	Diabase	Mafic dike in MNF	29°58.82′ N, 91°10.26′ E	Porphyric; ~60% groundmass of plagioclase, olivine and clinopyroxene (<~1 mm); ~40% phenocrysts of amphibole/clinopyroxene (~2–4 mm); overprinted with some chlorite and calcite.
LZ9912	Diabase	Mafic dike in LDF	29°57.89′ N, 91°07.52′ E	Porphyritic; ~80% groundmass of plagioclase, olivine and clinopyroxene (<~1 mm); ~20% phenocrysts of amphiboles/clinopyroxene (2–4 mm); altered and overprinted with chlorite and calcite.

indicate precision and accuracy better than 5% (2σ) for major elements and 10% (2σ) for trace elements. The analytical procedure in detail can be found in Rudnick et al. (2004).

Rb–Sr and Sm–Nd isotopic compositions were measured on a VG354 mass spectrometer at the Institute of Geology and Geophysics, Chinese Academy of Sciences, Beijing. Whole-rock powders (70–50 mg) were spiked with mixed isotope tracers, digested/dissolved in mixed acid (HF: $HClO_4$=3:1) in Teflon bombs for 7 days before chemical separation using AG50WX8 (H+) exchange columns. Analyses of NBS987 standard run during the same period gave $^{87}Sr/^{86}Sr=0.710214\pm11$ (N=10). Analyses of BCR-1 and La Jolla Nd standards gave $^{143}Nd/^{144}Nd=0.512602\pm10$ and 0.511841 ± 9 (N=12), respectively. All measured $^{143}Nd/^{144}Nd$ and $^{86}Sr/^{88}Sr$ ratios are fractionation corrected to $^{143}Nd/^{144}Nd=0.7219$ and $^{86}Sr/^{88}Sr=0.1194$, respectively. The analytical procedure in detail is given in Zhang et al. (2002) and Fan et al. (2003).

Table 3
Major and trace element abundances of representative samples from the Linzizong Volcanic Succession in Linzhou Basin, southern Tibet[a]

Formation	Lower Dianzhong Formation (LDF)					Middle Nianbo Formation (MNF)					Upper Pana Formation (UPF)					Mafic dykes	
Sample number	D-2	D-15	BD-145	BD-151	BD-160	BD-65	LZ9921	BD-55	L060	LZ994	LZ9917	LZ9916	BD-103	BD77	P-1	BD-58	LZ9912
SiO_2	59.16	58.05	61.57	57.46	58.77	49.69	74.69	74.01	77.64	71.56	75.58	79.64	67.93	68.98	74.06	43.33	44.68
TiO_2	0.7	0.68	0.62	0.64	0.71	0.92	0.13	0.12	0.12	0.46	0.3	0.31	0.36	0.25	0.17	0.99	0.99
Al_2O_3	16.02	15.92	15.88	18.04	17.11	17.08	12.03	11.78	11.42	12.4	11.21	9.75	13.56	18.09	13.33	15.62	16.37
TFe_2O_3	6.21	6.75	5.46	5.28	7.42	9.46	1.58	1.47	1.498	3.53	2.6	2.39	2.99	0.72	1.33	9.96	9.7
FeO	2.1	2.7	2.02	2.8	0.25	1.88	0.5	0.35	0.48	0.28	0.38	0.32	0.55	0.15	0.38	5.25	4.15
MnO	0.15	0.15	0.11	0.11	0.1	0.17	0.03	0.09	0.04	0.12	0.03	0.02	0.1	0.01	0.08	0.18	0.14
MgO	3.66	2.53	1.77	1.91	1.77	3.27	0.45	0.43	0.21	0.53	0.48	0.23	0.84	0.27	0.28	3.85	3.44
CaO	3.67	6.49	5.62	7.92	3.13	8.67	2.28	2.35	1.6	2.34	0.59	0.39	2.78	0.28	1.06	11.39	12.06
Na_2O	4.11	2.73	3.03	2.61	5.63	2.86	2.31	2.41	3.46	3.81	1.71	2.3	2.83	4.15	3.33	1.61	2.4
K_2O	2.39	1.88	2.35	1.20	2.49	2.6	2.52	3.9	1.72	2.41	5.55	3.68	4.6	5.26	5.43	2.3	1.39
P_2O_5	0.19	0.17	0.17	0.18	0.22	0.44	0.03	0.03	0.03	0.09	0.14	0.16	0.14	0.06	0.04	0.35	0.47
LOI	3.62	4.22	3.48	4.56	3.07	5.03	3.68	3.09	2.12	3.3	1.77	1.12	3.39	1.68	0.8	10.78	8.42
Total	99.88	99.57	100.06	99.91	100.42	100.19	99.73	99.68	99.86	100.55	99.96	99.99	99.52	99.75	99.91	100.36	100.06
Sc	15.3	15.2	13.3	12.6	11.8	16.3	6.74	6.35		5.37	4.2	2.48	5.66	3.28	2.5	20.4	19.2
Rb	41.4	51.5	63.1	21.8	71.3	53.2	81.4	105	81	59.9	163	88.7	123	123	198	62.1	29.9
Sr	450	386	351	436	566	1021	76.5	132	178	183	164	206	307	335	235	763	967
Y	23.3	23.3	22.1	23.3	22.7	39.3	24.3	29.5	35.5	17.8	17.7	13.7	21.4	28.9	17.8	27	28.5
Zr	136	118	129	156	134	149	95.6	114	112	117	113	101	150	234	142	118	145
Nb	7.04	5.39	7.29	6.14	5.88	10.8	7.56	8.56	11	7.48	8.67	7.88	12	19.4	11.9	7.94	10.1
Cs	0.71	1.53	1.61	2.36	5.55	1.97	3.33	1.85		4.9	13	8.16	4.34	2.61	2.31	4.55	3.23
Ba	965	354	428	390	392	1023	363	581	279	240	813	1304	745	919	691	636	586
La	21.7	19.8	22.3	20	19.9	48.2	33.7	31.9	40.9	28.6	38.3	28.2	40.3	62.9	36.6	34.5	48.8
Ce	44.9	39.7	45.3	41.4	38.7	87.9	64.7	63	88.8	60.5	60.7	44	72.8	105	65.3	69.7	106
Pr	5.47	4.73	5.3	5.17	4.93	11.1	8.12	7.24	10.9	7.31	8.24	6.21	8.04	12.4	6.72	8.44	12
Nd	22	19.1	21	21.8	21	45.9	29.6	27.7	34.7	27.4	29.1	23	28.5	42.5	22.9	36.2	51.3
Sm	4.58	4.25	4.44	4.78	4.61	9.29	5.67	5.71	7.58	5.11	5.32	4.27	5.51	6.74	4.1	7.88	9.73
Eu	1.23	1.1	1.12	1.24	1.22	2.33	0.58	0.72	1.09	0.97	1.1	0.96	1.21	1.48	0.75	1.99	2.58
Gd	4.57	4.3	4.58	4.82	4.65	9.02	4.58	5.96	6.95	4.15	4.02	3.24	5.61	6.92	4.22	7.77	8.38
Tb	0.66	0.66	0.68	0.71	0.7	1.11	0.68	0.9	1.12	0.62	0.57	0.46	0.73	0.88	0.55	1.03	1.28
Dy	3.91	3.94	3.94	4.17	4.02	5.69	4.31	5.23	5.88	3.97	3.47	2.51	4	4.82	3.11	5.39	6.26
Ho	0.8	0.82	0.8	0.85	0.82	1.01	0.89	1.08	1.27	0.79	0.6	0.49	0.76	0.95	0.63	1	1.04
Er	2.15	2.17	2.15	2.24	2.11	2.54	2.43	2.89	3.24	2.17	1.71	1.29	2.08	2.63	1.78	2.5	2.77
Tm	0.32	0.33	0.32	0.33	0.31	0.36	0.34	0.43	0.52	0.31	0.23	0.2	0.31	0.4	0.28	0.34	0.33
Yb	2.39	2.39	2.34	2.41	2.31	2.49	2.33	3.23	3.08	2.23	1.62	1.28	2.25	2.92	2.17	2.41	2.31
Lu	0.36	0.35	0.35	0.36	0.34	0.36	0.34	0.48	0.49	0.33	0.24	0.19	0.35	0.46	0.34	0.35	0.31
Hf	3.5	3.14	3.54	4.17	3.57	3.69	3.66	3.99	3.22	4.19	3.08	2.55	3.93	5.77	4.01	2.94	3.48
Ta	0.47	0.4	0.56	0.44	0.42	0.46	0.9	0.71	0.71	0.75	0.74	0.54	0.89	1.05	1.08	0.32	0.57
Th	9.17	9.32	11.1	9.1	7.65	13.9	16.5	19.1	13	14	21	13.2	27.7	24	35.3	9.1	9.86
U	1.88	1.85	2.32	1.99	1.42	2.08	3.66	3.24	2.85	2.7	4.23	5.48	6.23	6.13	6.76	1.48	2.44

[a] See text for analytical details.

5. Data

5.1. Major and trace elements

Major and trace element data (Table 3) on selected samples (Table 2) (Dong, 2002; Mo et al., 2003) confirmed the previous notion (Pearce and Mei, 1988; Jin and Xu, 1982) that the LVS rocks are mostly calc-alkaline although some are more alkalic, and can be further classified into several rock types on the TAS diagram (Fig. 2a). The Lower Dianzhong Formation (LDF) comprises ~50% lava flows and ~50% compositionally equivalent pyroclastic deposits (Table 1). The lavas are mostly andesite and trachy-andesite with minor basaltic andesite, and rhyodacite. Hornblende and plagioclase are common phenocrysts with minor clinopyroxene and some biotite in rhyodacite. Chemically, the samples plot mostly in calc-alkaline field in K_2O–SiO_2 space (Fig. 2b).

The Middle Nianbo Formation (MNF) comprises rhyolitic-dacitic tuffs, breccias and ignimbrites with layers of basaltic trachy-andesite and trachy-andesite with shoshonite present upper in the sequence (Table 1). Plagioclase and hornblende are common phenocrysts, and biotite become abundant at the top. Chemically, the MNF is diverse, and clearly bimodal in terms of SiO_2 contents. About 30% of the samples plot in the high-K field in K_2O–SiO_2 space (Fig. 2b).

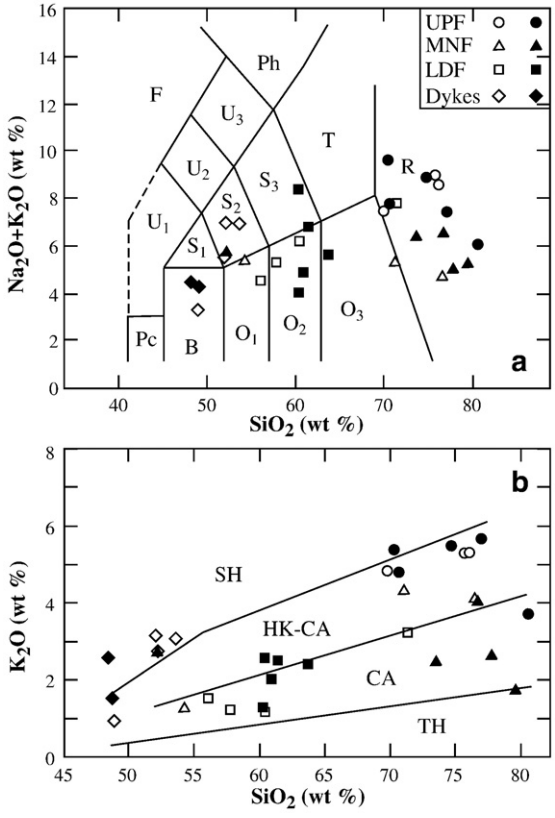

Fig. 2. Major element compositions of the lower Dianzhong (LDF), middle Nianbo (MNF), and upper Pana (UPF) formations plus mafic dykes of the Linzizong Volcanic Succession (LVS) from the Linzhou Basin in [a] K_2O+Na_2O vs. SiO_2 (after Le Bas et al., 1986) and [b] K_2O vs. SiO_2 (Rickwood, 1989) spaces. Open symbols are published data (Mo et al., 2007), and the solid symbols are new data of this study (Table 2). Symbols in [a] are: Pc, picrobasalt; B, basalt; O_1, basaltic andesite; O_2, andesite; O_3, dacite; R, rhyolite; S_1, trachy-basalt; S_2, basaltic trachy andesite; S_3, trachy-andesite; T, trachyte; U_1, tephrite/basanite; U_2, phono-tephrite; U_3, tephri-phonolite; Ph, phonolite; F, foidite. Abbreviations in [b] are: SH, shoshonitic; HK-CA, high potassic calc-alkaline; CA, calc-alkaline; TH, tholeiitic.

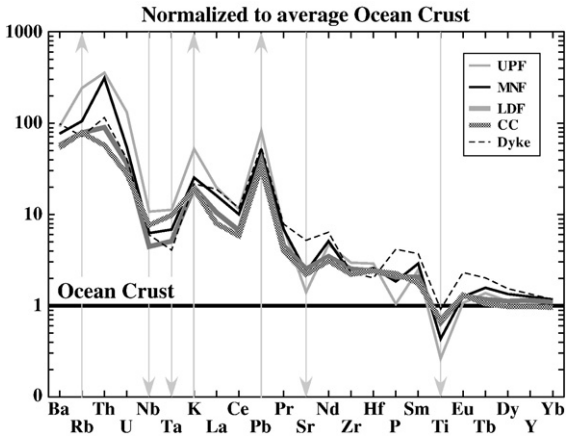

Fig. 3. Multi-element plots of the LVS rocks normalized against average composition of model ocean crust (Niu and O'Hara, 2003). Plotted are averages of the rhyolitic upper Pana (UPF, N=16), dacitic middle Nianbo (MNF, N=10) and andesitic lower Dianzhong (LDZ, N=15) formations plus mafic dykes (N=6). Bulk continental crust composition (CC, Rudnick and Gao, 2003) is plotted for comparison. Data used for averages are from Table 2, Mo et al. (2007) plus our unpublished data. The grey vertical lines emphasize relative depletion (downward arrows) of high field elements plus Sr and relative enrichment (upward arrows) of large ion lithophile elements of these rocks and progressively more so from LDF to MNF and to UPF.

The upper Pana Formation (UPF) is dominated by ignimbrites with abundant high-K breccias and rhyolite blocks (Table 1). Lava flows are less abundant. Chemically, the samples are rich in SiO_2, K_2O and Al_2O_3 (Fig. 2). About 80% of the samples plot in the high-K calc alkaline fields in K_2O–SiO_2 space (Fig. 2b). All these have been previously interpreted as reflecting large scale melting of thickened continental crust (Mo et al., 2002, 2003), perhaps genetically associated with the earlier LDF. There are also relatively late alkali-rich diabasic dykes (Fig. 2) intruded the upper section of the LDF, and acidic dykes intruded the upper section of the UPF (not shown).

Overall, the LVS rocks, in particular the more primitive andesitic LDF, broadly resemble average composition of the continental crust (Rudnick, 1995; Rudnick and Gao, 2003) (Fig. 3). They are enriched in the progressively more incompatible elements with characteristic "arc-like signature", i.e., depletion of Nb, Ta and Ti and enrichment of Pb, K and other large ion lithophile elements except for Sr that is not enriched, but slightly depleted (Fig. 3). Their heavy rare earth element abundances and patterns resemble those of oceanic and continental crusts without the so-called "garnet signature". However, the average compositions of the three formations (also the alkali diabasic dykes) differ in detail as elucidated in Fig. 4, where formation averages are used to emphasize first-order systematics.

Fig. 4 shows that over the ~20 Myr period (~65 to ~44 Ma), the LVS volcanism in the Linzhou basin exhibits, to a first order, a progressive change: andesitic → dacitic → rhyolitic in terms of

Table 4
Sr–Nd isotopic compositions of the representative samples from the Linzizong Volcanic Succession in Linzhou Basin, southern Tibet[a]

Sample number	Formation	Rb (ppm)	Sr (ppm)	$^{87}Rb/^{86}Sr$	$^{87}Sr/^{86}Sr$	$^{87}Sr/^{86}Sr(I)$[b]	Sm (ppm)	Nd (ppm)	$^{147}Sm/^{144}Nd$	$^{143}Nd/^{144}Nd$	$\varepsilon_{Nd(t)}$[c]
D-2	Dianzhong	42.06	477.4	0.255	0.705973	0.70577	4.274	20.97	0.1232	0.51259	−0.44
BD-27	Dianzhong	31.88	471.3	0.1958	0.706243	0.70609	3.962	18.26	0.1312	0.51248	−2.64
BD-123	Dianzhong	33.41	386.8	0.25	0.706451	0.70626	4.024	19.59	0.1243	0.51265	0.78
L1108	Dianzhong	20.56	646.23	0.0918	0.704668	0.70460	3.304	14.98	0.1333	0.51309	9.20
BD-55	Nianbo	113.8	124.3	2.649	0.709704	0.70763	5.498	28.69	0.1159	0.51264	0.61
LZ9921	Nianbo	87.17	80.3	3.142	0.709467	0.70701	5.318	27.29	0.1179	0.51260	−0.23
LZ9910	Nianbo	7.46	273.1	0.07905	0.707418	0.70736	8.1	38.43	0.1275	0.51273	2.32
BD-114	Pana	180	100.5	5.242	0.709848	0.70575	9.621	53.66	0.1084	0.51251	−1.88
BD-106	Pana	153.3	171.8	2.583	0.706705	0.70469	4.993	28.05	0.1076	0.51256	−0.95
P-1	Pana	222.1	247.1	2.601	0.70677	0.70474	4.096	24.19	0.1024	0.51245	−3.01

[a] See text for analytical details.
[b] $(^{87}Sr/^{86}Sr)I=(^{87}Sr/^{86}Sr)_{ROCK}-(^{87}Rb/^{86}Sr)_{ROCK}*(e^{\lambda t}-1)$, where $\lambda=1.42*10^{-11}$.
[c] $\varepsilon_{Nd(t)}=[(^{143}Nd/^{144}Nd)_{ROCK(t)}/(^{143}Nd/^{144}Nd)_{CHUR(t)}-1]*10{,}000$, where $(^{143}Nd/^{144}Nd)_{CHUR(t)}=(^{143}Nd/^{144}Nd)_{CHUR(present)}-(^{147}Sm/^{144}Nd)_{CHUR(present)}*(e^{\lambda t}-1)$, $(^{143}Nd/^{144}Nd)_{CHUR(present)}=0.512638$, $(^{147}Sm/^{144}Nd)_{CHUR(present)}=0.1967$, $\lambda_{Sm}=6.54*10^{-12}$, and $(^{143}Nd/^{144}Nd)_{ROCK(t)}=(^{143}Nd/^{144}Nd)_{ROCK(present)}-(^{147}Sm/^{144}Nd)_{ROCK(present)}*(e^{\lambda t}-1)$.

SiO_2 with associated changes in other elements that are consistent with progressively more evolved nature such as (1) weakened mafic character (first row panels), (2) elevated incompatible element abundances, particularly the sharp increase in alkalis (e.g, K and Rb) in the UPF (second row panels), and (3) advanced degree of crystallization/removal of liquidus phases such as titanomagnetite (Nb, Ta and Ti depletion), apatite (P depletion) and plagioclase (Sr and Eu depletion) (third row panels) as otherwise expected during mantle melting (Sun and McDonough, 1989; Niu and Batiza, 1997).

5.2. Sr and Nd isotopes

New Sr and Nd isotope data of the LVS rocks are given in Table 4, and plotted together with existing data (Mo et al., 2007)

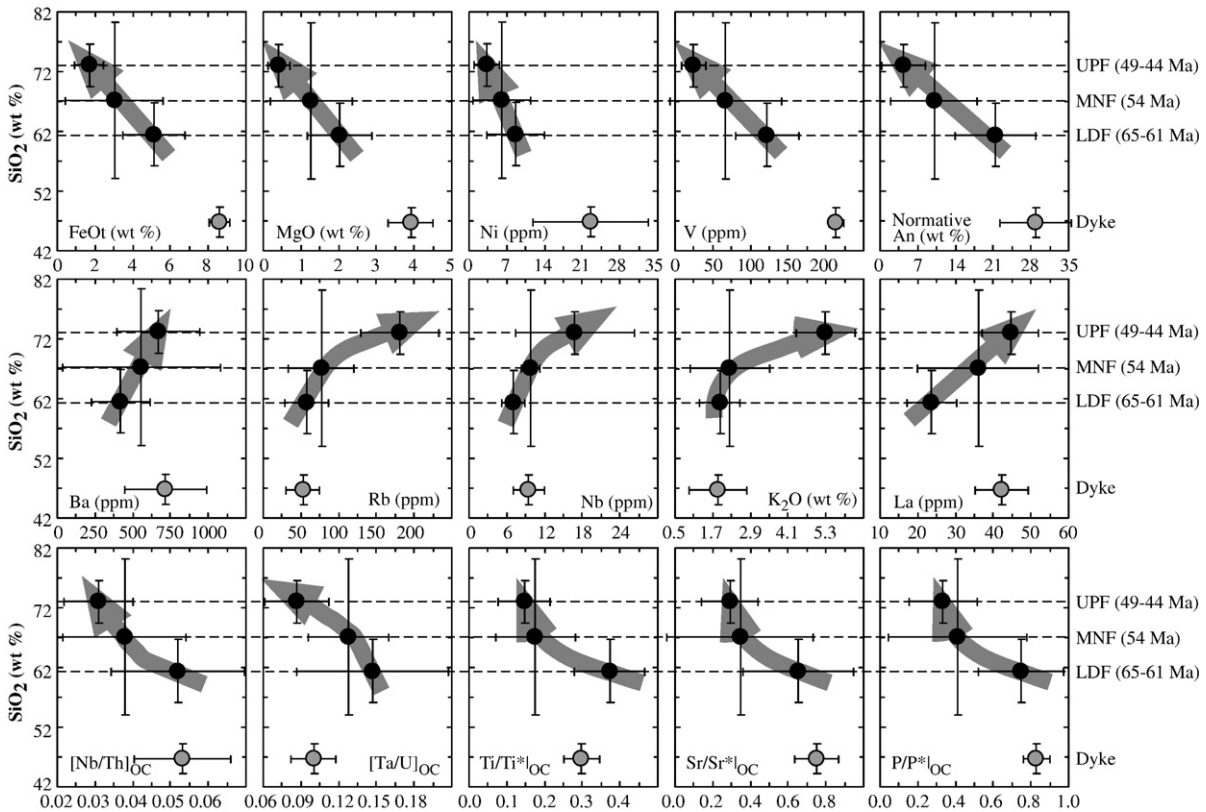

Fig. 4. Formation averages of representative elements and ratios plotted against SiO_2 stratigraphically upwards from lower Dianzhong (LDF), middle Nianbo (MNF) and upper Pana (UPF) formations plus mafic dykes. Error bars are $\pm 1\sigma$ from the means. The subscript OC refers to normalization against model ocean crust composition (Niu and O'Hara, 2003), where $Ti/Ti^*|_{OC}=(Ti/[Sm+Gd])_{OC}$, $Sr/Sr^*|_{OC}=(Sr/[Pr+Nd])_{OC}$, and $P/P^*|_{OC}=(P/[Nd+Sm])_{OC}$. Data sources are the same as in Fig. 3.

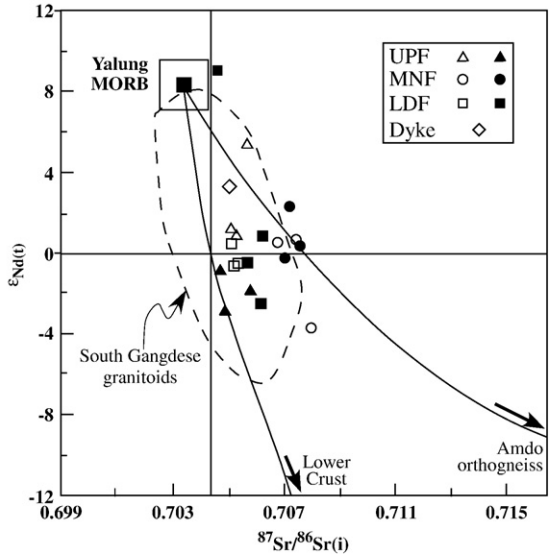

Fig. 5. In $^{87}Sr/^{86}Sr$ vs. $\varepsilon_{Nd(t)}$ space, representative samples from the three formations and mafic dykes (see Table 1 and Figs. 2–4) of the LVS show no systematic, but overlapping variations.. Open symbols are published data (Mo et al., 2007), and solid symbols are new data of this study (Table 3). Note the field of the SGB (after Hou et al., 2004; Mo et al., 2005; and our unpublished data) that encompasses/overlaps Sr–Nd isotopic compositions of the LVS. Yarlung MORB (interpreted to represent the Tethyan ocean crust; Mahoney et al., 1998), Amdo orthogenesis (interpreted to represent the upper crust; Harris et al., 1986), and a theoretical lower crustal composition (Ben Othman et al., 1984) are indicated for reference.

in Fig. 5, showing $\varepsilon_{Nd(t)}=-4.0$ to $+9.2$ and $(^{87}Sr/^{86}Sr)_i=0.704690–0.708316$, respectively. The field defined by the coeval SGB intrusives is highlighted to show the similar Nd–Sr isotopic variation range. Despite the varying Nd–Sr isotopic ratios, samples with $\varepsilon_{Nd(t)}>0$ require significant mantle contribution to the LVS (also the SGB) petrogenesis. Note that the three formations show no systematic, but overlapping, variations in Nd–Sr isotope space despite the more evolved (increasing SiO_2) bulk-rock major and trace element systematics stratigraphically upwards (Fig. 4), suggesting the possibility that the more evolved MNF and UPF may have in fact derived from melting of the earlier andesitic LDF — the most primitive LVS end-member (or intrusive equivalent).

Contributions from mature continental crust are apparent as a number of samples have $\varepsilon_{Nd(t)}<0$, and the overall data define a "cluster", trending towards crustal compositions represented by the Amdo orthogenesis (Harris et al., 1986; Dewey et al., 1988) and a hypothetical lower crust granulite (Othman et al., 1984). As mature continental crust must have significantly higher Sr and Nd abundances than mantle and mantle derived melts (e.g., the ocean crust), continental crust contribution is likely much less than mantle contributions (see below). Importantly, one of the UPF SiO_2-rich samples has a very high $\varepsilon_{Nd(t)}$ value (>+4; Fig. 5) whereas some less felsic LDF and MNF samples have lower $\varepsilon_{Nd(t)}$ values (<0; Fig. 5). This suggests that the crustal contribution to the LVS petrogenesis may not be simple crustal level assimilation, but probably occurs in the melting region. Melting of recycled terrigeneous sediments or subduction-eroded crustal materials is likely.

6. Discussion

6.1. Petrogenesis of the Linzizong Volcanic Succession (LVS)

To emphasize the first order observations and for convenience, we focus here on the origin of "primary magmas" parental to the intermediate/felsic rocks of the LVS (i.e., the andesitic LDF, dacitic MNF and rhyolitic UPF lava flows and pyroclastic rocks). Detailed studies of the coeval SGB intrusives (see Mo et al., 2005) are in progress, but we stress that the "primary magmas" that we wish to discuss here also apply to these intrusives (i.e., diorite, granodiorite, granite etc.). We advocate that the inferred "primary magmas" are andesitic (vs. basaltic) in composition.

6.1.1. Geochronological constraints

It is now accepted that the India–Asia collision began at ~≥65 Ma, and ended at ~40 Ma (e.g., Yin and Harrison, 2000; Flower et al., 2001; Mo et al., 2002, 2003, 2006, 2007) with convergence continuing to present. It follows that the syncolissional LVS volcanic rocks (65–44 Ma) and SGB intrusives (60–40 Ma; Mo et al., 2005) must be a magmatic response to the India–Asia collision (Mo et al., 2002, 2005, 2007). This rules out the LVS being genetically associated with either intra-oceanic island arcs or continental arcs in space and time in terms of standard models for subduction-related magmatism, but points to a genetic link between the magmatism and continental collision.

6.1.2. Volumetric and phase equilibrium constraints

The felsic LVS rocks and SGB intrusives are volumetrically significant, and widespread along much of the Gangdese Belt (Fig. 1). This association differs from island arc assemblages dominated by basaltic rocks derived from mantle wedge peridotite melting. Wet peridotite melting can produce andesitic melts (O'Hara, 1965; Kushiro et al., 1968; Hirose, 1997), but such andesitic melt must be rich in MgO (i.e., HMA) to be in equilibrium with mantle peridotite (Kelemen, 1995; Tatsumi, 2006). However, the andesitic LDF, the most primitive basal LVS formation, has MgO=2.01±0.85 wt.%, which is too low compared to HMA (~5–10 wt.%) (Kelemen, 1995; Tatsumi, 2006) with FeO/MgO=2.78±0.94, which is too high to be derivatives from HMA (<2) (see Tatsumi, 2006). Very low degree water-saturated melt could have low MgO, but the amount of such melt is volumetrically insignificant, and would solidify upon ascent and not reach the surface (Tatsumi, 2006), let alone to explain the voluminous andesitic LDF of the LVS. Therefore, partial melting of basaltic rocks or crystallization from voluminous basaltic magmas over an extended period of time is required to produce the volumetrically significant LVS and SGB in time and space.

Basaltic magma crystallization–differentiation (Bowen, 1928) can produce a variety of more evolved silicic magmas, but is incapable of producing large amounts. Hence, to produce voluminous andesitic melts (e.g., the LDF), partial melting of materials with basaltic composition is required, and to produce large amounts of the more felsic melts (e.g., the MNF and UPF), partial melting of materials with intermediate/felsic

compositions (e.g., andesitic, dacitic and compositionally equivalent sediments) is needed. The key question is what is available to melt and how to produce the andesitic magmas parental to the LVS (also the SGB intrusives) in response to the India–Asia continental collision.

6.1.3. Isotopic constraints on the basaltic source rocks

A common view is that the collision-induced crustal thickening leads to anatexis of deep crustal materials as they become deeply buried and heated, but the underlying subducting/underthrusting lithospheric slab during collision is a heat sink, thus making heat unavailable to warm up the deep continental crust for some extended time period. Radioactive heat accumulation is an even slower process for syncollisional magma genesis. Slab dehydration induced anatexis of existing crustal materials (Le Fort, 1988) is plausible. It is also plausible that convective lithosphere removal and asthenospheric upwelling (England and Houseman, 1989; England, 1993) may provide the heat for crustal melting and granitoid magma generation (Kapp et al., 2007). However, the three LVS formations (i.e., the LDF, MNF and UPF) have overlapping isotopic compositions with $\varepsilon_{Nd(t)}$ = −4.0 to +9.2 (−6 to +8 for the SGB intrusives) (Fig. 5) (also see Dong, 2002; Mo et al., 2003; X. Mo's unpublished data), indicating significant asthenospheric mantle contributions. Hence, the LVS and SGB magmatism did not originate from melting of thickened deep continental crust.

In the broad context of the India–Asia collision, possible basaltic source candidates in abundance are (1) recently accreted island arc complex and (2) the remaining part of the Tethyan ocean crust, i.e., the leading edge of the Indian plate. Partial melting of such basaltic rocks would produce the more felsic magmas parental to the LVS and SGB. Because such basaltic candidates were recently derived from the mantle for the Tethyan ocean crust or largely from the mantle for a presumed island arc assemblage, the mantle isotopic signatures of the LVS and SGB felsic rocks must be inherited from their basaltic source rocks. It is noteworthy that while the southern Gangdese is considered an Andean-type active continental margin, there is no evidence for the presence of an island arc system in the neo-Tethyan ocean before the India–Asia collision along the entire Gangdese Belt (Yin and Harrison, 2000). Furthermore, island arcs with positive topography should remain at high level during collision as ophiolite assemblages (Niu et al., 2003), but the well-studied ophiolite occurrences along the Yarlung–Zangbo suture are 120–180 Ma typical MORB crust associations (Zhang et al., 2005). In any case, melting of mafic/ultramafic deep arc crust cumulate, if there were any, could produce andesitic melt, but such melt would be too depleted to account for the observed geochemistry of the LDF (see below). Re-melting of the existing Andean-type arc crust would be possible, but it requires such crust to be dominated by basaltic rocks with minimal involvement of mature continental crustal materials in its histories in order to maintain the prominent asthenospheric mantle signatures (Fig. 5).

Hence, volumetrically significant and physically plausible basaltic source material available for generating andesitic magmas parental to the LVS (also SGB) would be oceanic crustal materials atop the subducting/underthrusting Tethys oceanic lithosphere. Partial melting of such basaltic crust can produce "primary" melts of andesitic compositions with inherited asthenospheric isotopic signatures. This is a strong constraint. The LDF may be derived from such "primary" melts of ocean crust melting. Melting of the more felsic materials including terrigenous sediments along with the subducting/underthrusting ocean crust can produce the more felsic melts. The MNF and UPF, in particular the latter, most likely result from re-melting of rocks equivalent to the older LDF because of their similar mantle (vs. crustal) isotopic signatures with similar degrees of crustal contribution.

6.1.4. Mechanism and condition of the Tethyan ocean crust melting

After a long debate, it has been the general view that the subducting oceanic crust is too cold to melt in subduction zones (e.g, Peacock, 2003). Melting of young (<25 Ma) and warm slabs has been a popular concept to explain rocks with adakite geochemical signatures (Defant and Drummond, 1990), but adakites and adakitic rocks can be produced through different means and in different environments without slab melting (Hou et al., 2004; Castillo, 2006; Guo et al., 2007; Mo et al., 2007). Nevertheless, there has been a recently renewed advocacy that melting of the subducting slab together with sediments is in fact required to explain the geochemistry in some arc lavas (e.g., Johnson and Plank, 1999; Kelemen et al., 2003c; Elliott, 2003; Mez-Tuena et al., 2007).

The foregoing discussion and reasoning suggest that melting of the Tethyan ocean crust is indeed required to account for the syncollisional LVS and SGB. The subducting/underthrusting Tethyan seafloor during the India–Asia collision must differ in physical conditions from slabs in active subduction zones. The ocean crust is known to have been highly hydrated before entering subduction zones because of near-ridge hydrothermal alteration and because of subsequent seafloor weathering. Melting of such hydrated basaltic crust occurs when it reaches the wet solidus of basaltic rocks (Fig. 6). Fig. 6 is a simplified phase diagram showing hydrous (H_2O-saturated) solidi of basalts and the more felsic lithologies (tonalite and granite, including terrigeneous sediments of similar compositions), three major metamorphic facies fields (eclogite, amphibolite and granulite facies), and two geothermal gradients approximating two extreme subduction zone scenarios: the cold subducting slab with a thermal gradient of ~5 °C/km, and a warm slab with a gradient of ~13 °C/km inferred from models of Peacock and Wang (1999). These model geotherms have been taken as indicating subduction zones being too cold to melt except when slabs are young (<25 Myrs old), warm and subducting slowly (Defant and Drummond, 1990), in which case the subducting ocean crust would evolve along a warm geotherm (e.g., the ~13 °C/km) and may melt in the eclogite stability field to produce adakites with the "garnet signature". The "garnet signature" offers a strong geochemical line of evidence for slab melting. Kelemen et al. (2003c) reviewed petrologic and seismic data indicating that *P–T* conditions

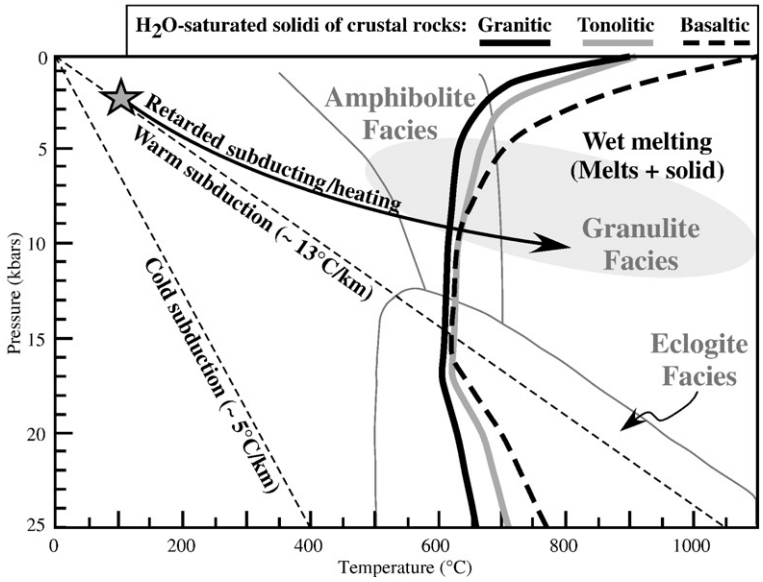

Fig. 6. Semi-quantitative phase diagram showing hydrous (H_2O-saturated) solidi of basalts and the more felsic lithologies (granite and tonalite) modified from Niu (2005) using the experimental data of Stern et al. (1975), Wyllie (1979), and Wyllie and Wolfe (1993). The three major metamorphic facies fields (eclogite, amphibolite and granulite) are drawn after Peacock (2003). The two geothermal gradients approximating two extreme subduction zone scenarios are inferred from models of Peacock and Wang (1999). The star and the solid line with arrow illustrates the concept of the subducted/underplating Tethyan ocean crust evolution along a high T/P path as a result of retarded subducting and enhanced heating upon and during India–Asia collision. It is expected that the highly hydrated (altered/weathered?) ocean crust begins to melt when intersecting the hydrous basaltic solidus under amphibolite facies conditions. Sediments of the more felsic compositions (i.e., granitic or tonalitic) will melt under similar conditions. H_2O-undersaturated solidus (i.e., amphibole-dehydration melting curves; Wyllie and Wolfe, 1993) is not shown for simplicity. The grey oval indicates P–T conditions, where melting can take place, beneath active arcs constrained by petrologic and seismic observations summarized by Kelemen et al. (2003c).

beneath many active arcs are in fact much hotter (e.g., the grey oval area with dT/dP=~20 to 50 °C/km in Fig. 6) than indicated by most model geotherms. They also argued that more realistic mantle wedge flow models considering temperature-dependent viscosity can well explain the thermal conditions constrained by petrologic and seismic observations. If slabs melt at these shallow levels of amphibolite (also "granulite") facies, the melt would have no "garnet signature" and thus offer no convincing geochemical evidence for slab melting, but melting can indeed take place in terms of straightforward phase relationships in Fig. 6.

We hypothesize here that the evolution path of the last part of the Tethyan ocean crust (star and the thick curve with arrow in Fig. 6) differs from a normal subducting slab. Upon India–Asia collision, the convergence continued, but the rate of Tethyan crust underthrusting must be retarded. The latter facilitates thermal equilibrium of the crust with the overlying mantle/crust, making the underthrusting crust evolve along a higher T/P geotherm, e.g, >>13 °C/km (Fig. 6). This hydrated underthrusting crust will inevitably melt when intersecting the hydrous basaltic solidus in the amphibolite facies (Fig. 6). We term this melting mechanism compression (vs. decompression) and equilibrium heating induced melting of H_2O-saturated basaltic rocks (Niu, 2005). Sediments of the more felsic compositions (e.g, granitic or tonalitic; Fig. 6) going along with the underthrusting Tethyan crust would melt under similar conditions (Nichols et al., 1994).

Note that melting of the hydrated Tethyan crust is physically straightforward. A geotherm of ~17 °C/km would mean ~680 °C at depth of ~40 km, which is already in excess of wet solidus of basaltic rocks (<650 °C, Fig. 6) to induce the underthrusting Tethyan crust to melt. In practice, it should take a few million years for the "cold" ocean crust to reach that wet solidus. Assuming a convergence rate of ~50 mm/yr and slab dipping of ~30° upon collision, it would take ~1.6 Myrs for the Tethyan ocean crust to reach the depth of ~40 km. Because the Tethyan crust underthrust beneath/against the warm crust/lithosphere of the prior hot continental arc, the geotherm must be >20 °C/km well within the melting conditions (Kelemen et al., 2003c). It is possible and likely that the Tethyan crust can reach temperature in excess of 800 °C with continued underthrusting to produce significant amounts of melt. This concept is illustrated schematically in Fig. 7. Note that we stress ~40 km, not deeper, because LVS rocks lack "garnet signature" (see Fig. 3 and also below).

6.1.5. Chemical properties of "slab melts" formed in the amphibolite facies

Melts produced from such unusually "warm slabs" in the amphibolite facies (1) would be andesitic or more silicic, depending on the extent of melting and amount of sediments melted; (2) would have mantle (vs. crustal) dominated isotopic signatures inherited from the ocean crust (MORB-like); (3) may show no garnet signature (vs. adakitic) because garnet is not a stable phase under <1.0 GPa subsolidus conditions of the basaltic source assemblage (Wyllie and Wolfe, 1993; Wolf and Wyllie, 1994; Vielzeuf and Schmidt, 2001), nor a peritectic phase during melting (Wyllie and Wolfe, 1993); (4) would have

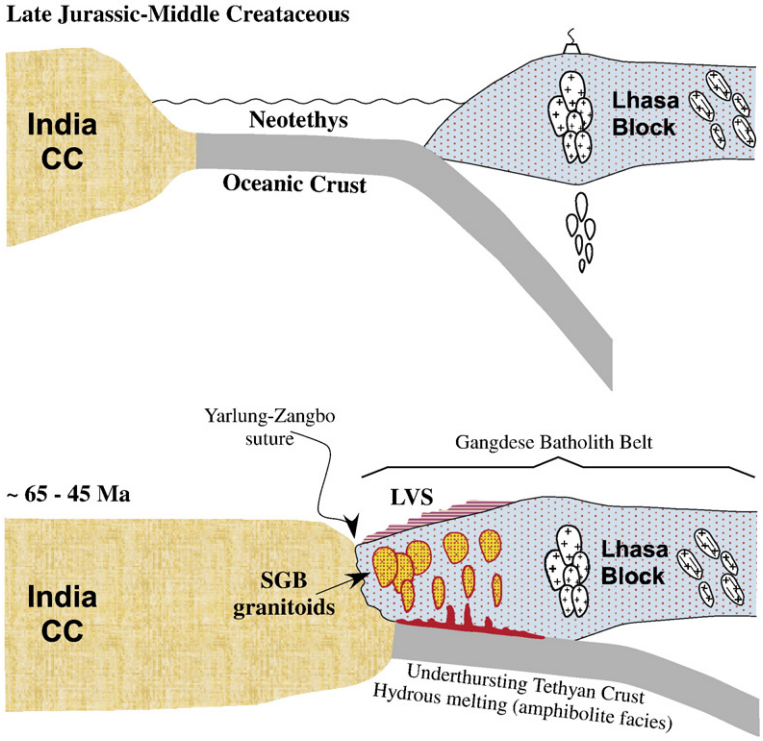

Fig. 7. Top: cartoon, showing the Tethyan Ocean with passive continental margin in Indian plate and Andean-type margin at the edge of the Lhasa block (Gangdese Belt) prior to the collision based on data from Yin and Harrison (2001). Bottom: Cartoon illustrating the concept of Tethyan ocean crust melting to produce syncollisional andesitic melts parental to the LVS and SGB (also see Fig. 6).

"arc-like signature", i.e., relative depletion in Nb, Ta and Ti because these high-field strength elements (HFSE) are compatible in ilmenite (or pseudobrookite), which is a common phase in amphibolite (Niu and Lesher, 1991) and its refractory property make it a residual phase holding these elements; (5) would have sub-chondritic Nb/Ta ratio because of amphibole-controlled fractionation ($Kd_{Nb}^{amp/L} > Kd_{Ta}^{amp/L}$) (Tiepolo et al., 2000; Foley et al., 2000, 2002; also see below); and (6) would not have excess Sr (vs. adakitic and arc magmas) (Fig. 3) because of calcic plagioclase as a residual phase preferentially holds Sr and Eu relative to Nd, Sm, Gd and other otherwise similarly incompatible elements.

Indeed, the LVS volcanic rocks have all these properties (Figs. 3–5). The scatter in the Nd–Sr isotope space (Fig. 5) is likely caused by "mixing" of mature crustal materials (e.g., recycled sediments, subduction-eroded materials, crustal assimilation) with the Tethyan ocean crust (altered MORB) with inherited isotopically depleted MORB mantle signature in the recent past. Using the Amdo gneiss composition as the crustal end member and Yalung MORB as the mantle component (Fig. 5), the LVS volcanic rocks would have 70–90% mantle contribution in terms of Nd crustal index (NCI) of Depaolo et al. (1985): $NCI = [\varepsilon_{Nd\ (rock)} - \varepsilon_{Nd\ (M)}]/[\varepsilon_{Nd\ (C)} - \varepsilon_{Nd\ (M)}] = 0.1-0.3$ (Mo et al., 2007). Contribution of mature crustal materials is also apparent from trace elements such as the Rb, K and Pb spikes in Fig. 3. The negative Nb, Ta and Ti anomalies are conspicuous, the negative Sr anomaly is weak, but discernable, and the lack of garnet signature (i.e., flat Dy–Yb pattern) is obvious. In contrast to the chondritic Nb/Ta ~17.57 (e.g., Sun and McDonough, 1989), the LVS andesites have a mean sub-chondritic Nb/Ta ratio of ~13.

It is important to note that similar to average continental crust (Rudnick and Gao, 2003), the andesitic LDF of the LVS shows slight Sr depletion or negative Sr anomaly (relative to Pr and Nd; see Figs. 3 and 4), which contrasts arc magmas (Elliott, 2003; Niu and O'Hara, 2003) with slight Sr enrichment or positive Sr anomaly (relative to Pr and Nd). As altered ocean crust is enriched in Sr (Staudigel, 2003), Sr as a soluble element of the dehydrating slab contributes to arc magmas. In amphibolite, Sr is stabilized in plagioclase, and progressive melting facilitates Sr (also Eu) retention in the more calcic plagioclase while Pr, Nd and other otherwise similarly incompatible elements enter the melt. This supports our interpretation that bulk composition of continental crust may be genetically associated with syncollisional melting of "trapped" oceanic crust in the amphibolite facies (vs. slab-dehydration induced mantle wedge melting for arc magmatism).

The concept of "amphibolite-facies" slab (plus terrigeneous sediments) melting explains all the features of the LVS lithologies well. It is particularly straightforward to explain all the LDF and the SiO_2-poor samples of the MNF. Conceptually, the more evolved MNF and UPF could be produced by "differentiation-crystallization" from the LDF, but this is unlikely both volumetrically and chronologically (Table 1). Given the similar Sr–Nd isotopic variability in the three formations with progressively stronger mantle signature in the less "contaminated" samples (Fig. 5), we suggest that it is more plausible that both MNF and UPF may in fact have derived from

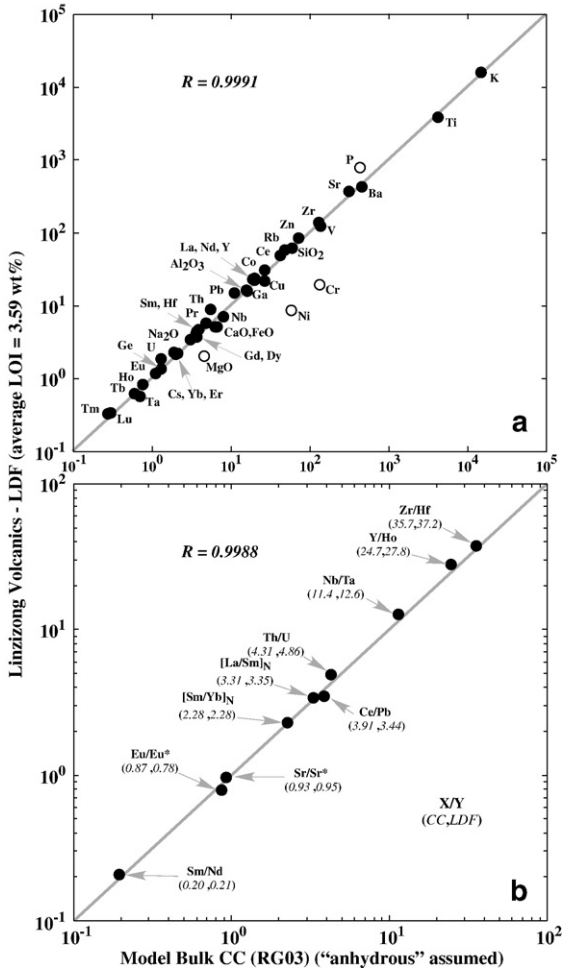

Fig. 8. Average composition of the most primitive LVS, i.e., the andesitic lower Dianzhong formation (LDF; N=22 for major elements and 15 for trace elements), shows remarkable similarity to the model continental crust composition (CC) of Rudnick and Gao (2003) on one-to-one plot in terms of [a] abundances of all the analyzed major and trace elements with the exception of P and compatible elements (or oxides) such as MgO, Ni and Cr (open circles), and [b] characteristic elemental ratios, including Eu/Eu* $(Eu/[Sm+Gd])_N$, Sr/Sr* $(Sr/[Pr+Nd])_N$, $[La/Sm]_N$) and $[Sm/Yb]_N$ where subscript N refers to normalization against primitive mantle values (Sun and McDonough, 1989). The log scale is used to show all the data with varying abundances (>5 orders of magnitude in [a]) and ratios (about 3 orders magnitude in [b]) such that degrees of deviations from the one-to-one line are of equal significance both visually and quantitatively. SiO_2, Al_2O_2, FeOt, MgO, CaO and Na_2O are in wt.%, and all other elements in ppm. Data are from Table 2, Mo et al. (2007) plus our unpublished data.

melting of the earlier lithologies, i.e., the LDF (and intrusive equivalent).

The volumetrically small but more mafic (MgO ~4 wt.%) diabasic dykes are not simply solidified primitive melt, but represent snapshot (frozen) of trachy-basaltic/andesitic melts with cumulate amphibole phenocryst (Yue and Ding, 2006). They share a common origin with the bulk LVS rocks in having similar Nd–Sr isotopes (Fig. 5) and similar trace element systematics (Fig. 3). The more mafic composition (Figs. 2 and 4) with the super chondritic Nb/Ta~21 and $[Dy/Yb]_N$>1 (Fig. 3) is consistent with amphibole accumulation.

6.1.6. More on the collision-associated andesitic magma genesis

If our interpretation above is correct, then the ~65–45 Ma LVS (and the coeval SGB) may reflect the active role or life span (~20 Myrs) of the last subducted bit of the Tethyan ocean crust during the collision. This inference is supported by the fact that there was a ~15 Myr (~40 to 25 Ma) magmaticaly quiescent period, though tectonically still active with significant compression and crustal thickening, before the post-collisional adakitic and ultra-potassic magmatism from ~25 Ma to 10 Ma, which are of entirely different origins (Mo et al., 2007; Guo et al., 2007). The lack of garnet signature in the LVS place the constraint that the depth of our perceived "amphibolite facies slab-melting" is shallow, <~40 km, where garnet is not a stable phase in the subsolidus conditions, nor a peritectic phase during melting (Wyllie and Wolfe, 1993; Vielzeuf and Schmidt, 2001). Ilmenite (or pseudobrookite), which is one of the primary hosts of Ti, Nb and Ta, is a common mineral in amphibolite (Niu and Lesher, 1991). It is likely to be a residual phase during melting because of its refractory nature, which readily explains the observed Nb–Ta–Ti depletion in the melts (Fig. 3). This, together with the involvement of recycled sediments as evidenced by the Nd–Sr isotopic data (Fig. 5), accounts for the "arc-like signature" (except Sr for reasons discussed above) (Fig. 3) without actually requiring active subduction zones.

6.2. Net contribution of syncollisional andesitic magmatism to continental crust mass

The LVS, in particular the andesitic LDF (Fig. 4), shows remarkable similarity in both abundances and systematics of incompatible elements to model bulk continental crust established using a comprehensive global approach (Rudnick and Gao, 2003) (Fig. 3). Fig. 8a compares all the analyzed elements (major, minor and trace elements) on one-to-one plot between average (N=22 for major and 15 for trace elements; including unpublished data) andesitic LDF and continental crust (Rudnick and Gao, 2003). The similarity between the two is striking with the exception of higher P and lower MgO, Ni and Cr in the andesitic LDF. What is more striking is the similarity between the two in terms of some key incompatible trace element ratios (Fig. 8b). The similar rare earth element (REE) abundances (Fig. 8a) and La/Sm, Sm/Nd and Sm/Yb ratios (Fig. 8b) point to the essentially identical REE patterns of the two without the so-called "garnet signature" (i.e., no heavy REE depletion; Fig. 3). Also note that both have similar negative Sr and Eu anomalies, which is consistent with amphibolite melting with plagioclase as a residual phase that stabilizes Sr and Eu relative to Pr, Nd, Sm, Gd and other otherwise similarly incompatible elements.

The model bulk continental crust composition by Rudnick and Gao (2003) is the most up-to-date painstaking effort built on works of generations (e.g., Taylor, 1967, 1977; Taylor and McLennan, 1985, 1995; Wedepohl, 1995; Rudnick and Fountain, 1995; Rudnick, 1995; Gao et al., 1998) using combined methods of petrology, geochemistry and geophysics on representative samples characterizing upper, middle and lower crust worldwide as well as sophisticated statistics and

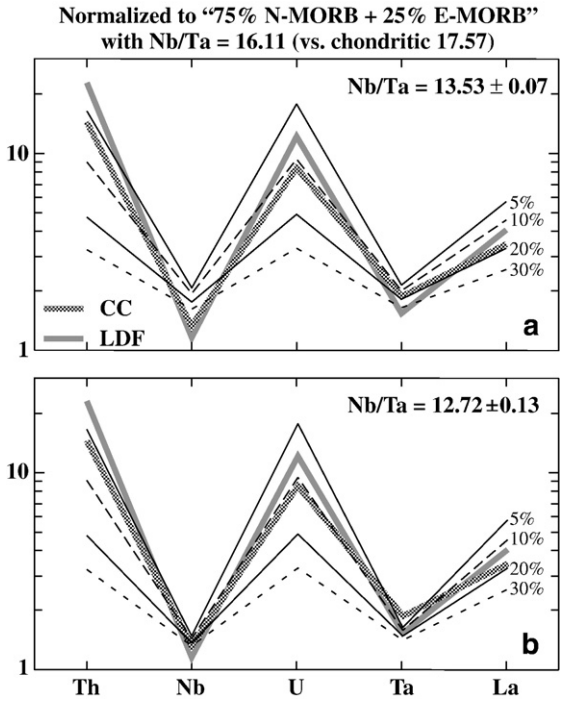

Fig. 9. Simple batch melting calculations to show the effectiveness of our suggested model of ocean crust melting at amphibolite facies conditions for the andesitic LDF of the LVS and model continental crust composition (CC; Rudnick and Gao, 2003) for key elements (Th, Nb, U, Ta, La and Nb/Ta). Both LDF andesite and CC are normalized against average MORB with 75% N-MORB and 25% E-MORB (Niu and O'Hara, 2003). Simplified mineral modes of the amphibolite of MORB protolith are taken from Niu and Lesher (1991): 66.4 wt.% "hornblende" (including minor chlorite, biotite and epidote), 4.4 wt.% ilmenite and 29.2 wt.% "plagioclase" (also including quarts and minor calcite). Partition coefficients between these major phases and basaltic andesite/andesite are: $Kd_{Nb}^{ilm/L}=3.45$ and $Kd_{Ta}^{ilm/L}=4.65$ (Green and Pearson, 1987); $Kd_{Th}^{ilm/L}=Kd_{U}^{ilm/L}=Kd_{La}^{ilm/L}=0$ (assumed); $Kd_{Nb}^{amp/L}=0.46$ and $Kd_{Ta}^{amp/L}=0.35$(Tiepolo et al., 2000); $Kd_{Th}^{amp/L}=0.0015$ and $Kd_{U}^{amp/L}=0.008$ (Brenan et al., 1995);$Kd_{La}^{amp/L}=0.18$, $Kd_{Nb}^{"plag"/L}=Kd_{Ta}^{"plag"/L}=Kd_{U}^{"plag"/L}=0.005$, and $Kd_{La}^{"plag"/L}=0.04$ are from various sources summarized in Niu et al. (1996). [a] 5%, 10%, 20% and 30% batch melting of the chosen "MORB" source reproduces the CC and LDF quite well, especially for 5% and 10% melting given the simplicity of the calculations and many unknowns. Note the more sub-chondritic Nb/Ta = 13.53 (vs. 16.1 of the source) because $Kd_{Nb}^{amp/L}/Kd_{Ta}^{amp/L}=0.46/0.35>1$ and because of high modal amphibole (66.4 wt.%) in the source rock. [b] Results after an arbitrary change of $Kd_{Nb}^{ilm/L}=Kd_{Ta}^{ilm}=8$ to better match Nb and to emphasize the influence of amphiboles on sub-chondritic Nb/Ta = 12.72. See text for details.

averaging procedures. Therefore, Figs. 3 and 8 proves two important points: (1) despite complex and heterogeneous lithologies in the continental crust, the model bulk crustal composition (Rudnick and Gao, 2003) is a robust representation of the continental crust; (2) syncollisional felsic magmatism, such as represented by the more mafic andesitic LDF of the LVS (and SGB) in southern Tibet, makes a genuine contribution to the mass of continental crust as they represent juvenile crustal materials derived from the mantle source in no distant past through a transitory stage of ocean crust formation.

The apparent depletion in highly compatible elements like Mg, Ni and Cr in the average LDF andesitic lithologies is a typical feature for andesites as noted by Taylor and McLennan (1985). High magnesian andesites have been put forward as ideal candidates for making continental crust because they have elevated Mg, Ni and Cr relative to the more common andesites (Kelemen, 1995; Tatsumi, 2006). We suggest here, however, that the "missing" Mg, Ni and Cr in syncollisional andesites are complemented by mafic and ultramafic lithologies (added oceanic plateaus, flood basalts, komatiites, ophiolites etc.) in the continental crust whose lower abundances of incompatible elements may modify, but cannot compensate the elevated abundances and systematics of incompatible elements in the bulk crust (Figs. 3, 4, 8). To quantify the elemental budget is beyond the scope of this current paper, which requires a large data set from the entire LVS and SGB that we collected in 2006 and are currently under investigation.

6.3. Zones of continental collision — the sites of mantle derived materials processed into andesitic crustal composition

In the standard "andesite" or "island arc" model for continental crust accretion, intra-oceanic volcanic arcs are required because of the understanding that the "arc-like signature" (Fig. 3) of continental crust originates from arc volcanism (e.g., Taylor and McLennan, 1985). In recent years, "oceanic plateaus", interpreted to result from episodic mantle plume activities, are considered to be important in crustal mass addition (Stein and Hofmann, 1994; Abbott and Mooney, 1995; Abbott et al., 1997; Polat et al., 1998; Albarède, 1998; Condie, 2000; Niu et al., 2003), and in explaining model age "spikes" preserved in the geologic record (McCulloch and Bennett, 1994; Condie, 2000). Assuming these two types of contribution are necessary, then closing of ocean basins with subduction zones is required to amass the intra-oceanic arcs and "scattered" oceanic plateaus to the growing continent.

However, if crustal production (magmatism) and loss (through subduction erosion and sediment recycling) at modern subduction zones, both intra-oceanic and Andean-type, is mass balanced (von Huene and Scholl, 1991; Scholl and von Huene, 2004; Clift and Vannucchi, 2004), and if crustal recycling at subduction zones has been important since ~2 Ga (Kramers and Tolstikhin, 1997), then active subduction zones may not have been the major sites of crustal growth. If oceanic plateaus are indeed important mass contributors to crustal growth (e.g., Abbott and Mooney, 1995), then the question remains (1) how has the continental crust developed its andesitic composition, and (2) where has the continental crust inherited its "arc-like signature"?

Following our foregoing discussions, we suggest that syncollisional felsic magmatism may in fact be the major mass contributor to crustal growth. For example, both LVS and SGB are volumetrically significant. Their andesitic composition (i.e., the most mafic LDF, which is likely to be the source rock for the more felsic MNF and UPF) may have resulted from partial melting of the remaining part of the Tethyan ocean crust, from which the LVS and SGB inherited the mantle isotopic signatures (Fig. 5; see also Mo et al., 2007). The latter affords evidence of the LVS and SGB being materials of the juvenile crust. As the syncollisional process of juvenile crust formation derives magmas from the ocean crust atop the subducting/

underthrusting oceanic lithosphere within the mantle, the more mafic residue of ocean crust melting remains in the mantle, which circumvents the need of the otherwise unknown process (es) to convert the more mafic arc assemblage to the andesitic continental crust required by the standard "island arc" model. Partial melting of the ocean crust at conditions of ≤~40 km not only explains the lack of "garnet signature", but also the characteristic "arc-like signature" (except for Sr; see above) in the melt parental to the LVS and SGB. The residual ocean crust after melt extraction will continue to enter the deep mantle along with the subjacent oceanic lithosphere.

Therefore, zones of continental collision are ideal sites of juvenile crust formation and continental crust accretion. We use the syncollisional LVS (and the coeval SGB) in southern Tibet to illustrate the concept, but similar observations have in fact been documented for the giant (>500,000 km^2) Central Asian Orogenic Belt (CAOB; from Central-Northern Mongolia to Transbaikalia, and from Kazakhstan, Xinjiang, through southern Mongolia, Inner Mongolia to NE China), where hundreds of Paleozoic to early Mesozoic age granitoid batholiths are widely distributed, many of which having $\varepsilon_{Nd(t)}>0$ (Jahn et al., 2000a, b). We speculate the CAOB granitoid batholiths must have formed the same way as we perceive for southern Tibet.

6.4. An efficacy test of our hypothesis

We have interpreted that the Paleogene felsic magmatism along the Gangdese Belt in southern Tibet as resulting from partial melting of the final bit of the Tethyan ocean crust in response to the India–Asia continental collision in terms of straightforward tectonic analysis, geological observations, geochemical arguments and petrologic concepts. Given the fact that our interpretation concerns the fundamental problem of where and how mantle derived melts contribute to continental crustal mass; it is necessary to test the interpretation fully quantitatively in terms of thermal and geochemical models. The debate on whether subducting slabs in active subduction zones can melt or not over the past decades (see Peacock, 2003; Kelemen et al., 2003c), for example, suggests that any convincing thermal model on whether trapped ocean crust can melt or not during continental collision is still distant, although simple physical arguments and phase relationship analysis (Fig. 7) suggests that such melting is more than likely.

Fully quantitative geochemical modeling is also remote because existing melting experiments on amphibolite or similar rocks are limited to phase stability, which does not allow quantitative parameterization of the melting reactions and melting mode proportions necessary for both major element and trace elements modeling. However, simple batch melting calculations with reasonable assumptions can be done to illustrate that partial melting of amphibolite of ocean crust protoliths can reproduce the first-order systematics of observed trace elements of the andesitic LDF of the LVS and the model continental crust (Rudnick and Gao, 2003). Fig. 9 shows our attempt by focusing on key elements (Th, Nb, U, Ta, La and Nb/Ta) that capture the critical feature of the continental crust. In calculations, we choose a combined "75% N-MORB+25% E-MORB" (Niu and O'Hara, 2003) as source rock, i.e., we normalized the andesitic LDF and model continental crust against this chosen MORB source in Fig. 9. This choice is based on the fact that statistically about 25% of MORB with $[La/Sm]_N>1$ and 75% with $[La/Sm]_N<1$ (Niu et al., 1999, 2001, 2002a). Note that bulk ocean crust (Niu and O'Hara, 2003) is too depleted as the source to explain the observations, which is interesting and important (i.e., gabbroic lower ocean crust is too depleted; Niu et al., 2002b). Amphibolite mineral modes of MORB protoliths (Niu and Lesher, 1991) and published experimental partition coefficients are used for the calculations (see caption to Fig. 9 for details). The negative anomalies of Nb and Ta with respect to Th, U and La are easily produced with ilmenite (or pseudobrookite) and amphibole as residual phases, and sub-chondritic Nb/Ta ratio is a straightforward result because $Kd_{Nb}^{amp/L}>Kd_{Ta}^{amp/L}$ and because of high modal amphibole (~66.4 wt.%) and low modal ilmenite (only 4.4 wt.%) despite $Kd_{Nb}^{ilm/L}\le Kd_{Ta}^{ilm/L}$.

Fig. 9a shows that 5%, 10%, 20% and 30% batch melting of the chosen MORB reproduces the CC and LDF reasonably well, especially for 5% and 10% melting, given the simplicity of the calculations because of many unknowns. Note that the more sub-chondritic Nb/Ta=13.53 (vs. 16.1 of the source). Fig. 9b shows results after an arbitrary change of $Kd_{Nb}^{ilm/L}=Kg_{Ta}^{ilm}=8$, which is not unreasonable given the uncertainties of published Kd values, to better match Nb and to emphasize the effect of amphiboles on sub-chondritic Nb/Ta=12.72. It is important to note that these results do not in any way mean that both LDF and CC are produced by 5–10% melting of amphibolite of a MORB protolith, but do emphasize the efficacy of our hypothesis. The models should match the data much better when considering involvement of terrigeneous sediments that will elevate Th, U and La. In fact, we anticipate ~15 to 30% melting to explain major element compositions and volumes of the melt produced.

To quantitatively evaluate the mass of the juvenile crust produced is not straightforward. Nevertheless, some rough estimates can be done. We assume (1) only the andesitic LDF (and equivalent intrusive portions) is melting product of the underthrusting Tethyan ocean crust (i.e., the dacitic MNF and rhyolitic UPF are melting derivatives from the LDF; see above); (2) a convergence rate of ~50 mm/yr (or 50 km/Myr) over the ~5 Myr period for the andesitic LDF; (3) only the upper ~3 km basaltic portion of the 7 km crust (i.e., basalts and sheeted dykes vs. lower crustal gabbros and cumulate) is involved in melting (see above); (4) the extent of melting is 30%; and (5) andesite is about 3% less dense than basalt, then we obtain 5 Myr * 50 km/Myr * 3.0 km * 0.3 * 1.03 = 232 km^3 andesitic crust per km strike length produced in this 5 Myr period. That is, the andesitic crust production rate is ~46 km^3 km^{-1} strike length per Myr. By assuming 30% melting of the upper ~4 km ocean crust, we would get ~62 km^3 km^{-1} strike length per Myr. If we apply this rough production rate to the entire 1500 km south Gangdese Belt, there would be ~348,000 km^3 to 464,000 km^3 juvenile andesitic crust. These estimates are to a first order consistent with the rough (not well-constrained) estimated volume of ~350,000 to 500,000 km^3 for the LVS and SGB combined.

It is interesting to note that the melt production rate of ~46 to 62 km^3 km^{-1} strike length per Myr is 1.5 to 2 times greater than the model average of ~30 km^3 km^{-1} arc strike length/Myr for Phanerozoic arc-crust production (e.g., Reymer and Schubert, 1984). This comparison may be less relevant because the syncollisional magmatism is short-lived whereas arc crust production at active subduction zones is long-lived and steady state. However, the latter is shown to be mass balanced by subduction erosion and sediment recycling (von Huene and Scholl, 1991; Clift and Vannucchi, 2004), whereas the syncollisional magmatism, along with the intra-oceanic plateaus trapped during collision, maintains net growth of the continental crust. We emphasize that precise estimation of juvenile crustal growth rate by syncollisional felsic magmatism requires a better understanding of melting processes by means of well-controlled melting experiments of amphibolite with MORB protolith to establish melting reactions with correct melting mode coefficients as a function of *P–T* conditions and water contents while paying attention to accessory phases and trace element partitioning.

7. Summary

1. The Linzizong volcanic rocks (~65–45 Ma) and the coeval ~60–40 Ma granitoids are dominant magmatic rocks distributed along much of the >1500 km long Gangdese Belt immediately north of the India–Asia suture (Yarlung–Zangbo) in southern Tibet (Fig. 1). They represent a magmatic response to the India–Asia continental collision as it progressed from a "soft" touch at ~70/65 Ma to a "hard" clash at ~45/40 Ma.
2. Our study of these rocks, primarily the LVS rocks from the Linzhou Basin near Lhasa (Fig. 1), shows that the syncollisional magmatism is broadly andesitic to rhyolitic in composition (Fig. 2) with a first-order temporal variation from the andesitic LDF (64.4–60.6 Ma), to the dacitic MNF (~54 Ma), and to the rhyolitic UPF (48.7–43.9 Ma) in terms of SiO_2 content with corresponding bulk rock major and trace element variations (Figs. 3 and 4).
3. All three formations show no systematic but overlapping Nd–Sr isotope variations (Fig. 5) despite the first-order bulk-rock compositional systematics (Fig. 4). The isotopically depleted end-member with $\varepsilon_{Nd(t)}>0$ substantiates that their primary sources are of mantle (vs. continental crust) origin.
4. The large volumes and vast spatial distribution of these felsic rocks preclude their being derived from melts of mantle peridotites, but are consistent with melting products of basaltic source rocks. The isotopically depleted mantle signature substantiates that the basaltic source rocks must have been derived recently from the asthenospheric mantle. In the broad context of Tethyan ocean closing and India–Asia collision, the remaining bit of the Tethyan ocean crust is the best source candidate.
5. The Tethyan ocean crust, upon collision, would subduct/underthrust slowly, tend to attain thermal equilibrium with the superjacent warm Andean-type arc lithosphere, and thus evolve along a high *T*/*P* path in *P–T* space. The warm hydrated ocean crust would melt when reaching the hydrous basaltic solidus in the amphibolite facies to produce andesitic melts parental to the LVS and SGB.
6. Ilmenite (or pseudobrookite) is a common phase in amphibolite of MORB protolith, and its refractory nature makes it a residual phase during melting that preferentially hosts Ti, Nb and Ta, which, combined with the influence of amphibole, accounts for the depletion of these elements in the melt. Residual amphibole that possesses super-chondritic Nb/Ta ratio explains the sub-chondritic Nb/Ta ratio in the melt (Fig. 9). Residual calcic plagioclase explains the small but discernible negative Sr anomaly in the melt (Figs. 3,8). Involvement of recycled mature crustal materials (e.g., terrigeneous sediments) plus effects of seafloor alteration enhances the abundances of elements such as Ba, Rb, Th, U, K and Pb. The lack of garnet signature in the melt is consistent with the high T/P evolution path where garnet is not a stable phase (Fig. 6). Hence, the characteristic "arc-like signature" can be developed this way without requiring processes of active subduction zones.
7. Therefore, we propose that continental collision zones are ideal sites of net crustal growth through process of syncollisional felsic magmatism. While our interpretations are reasonable in terms of straightforward petrology, geochemistry and tectonics, they can be refined with well-controlled amphibolite melting experiments as well as detailed studies of samples with greater spatial coverage along the entire Gangdese Belt.

Acknowledgements

This study was supported by Chinese Ministry of Science and Technology (2002CB41260), Chinese National Natural Science Foundation (40172025, 40103003, 40473020, 40572048, 40672044, 49772107, and 49802005), Chinese Ministry of Land and Resources (2003009), and the Chinese 111 Project (No. B07011). YN thanks the Royal Society for support through China-UK Science Networks programme and China University of Geosciences (Beijing) for a Lecturer Professorship. Discussion with Jon Davidson, Jim Gill, Mike O'Hara and Peter Wyllie was useful. The paper benefited from the thorough review and constructive comments by Susan DeBari, Roberta Rudnick and an anonymous reviewer. Roberta Rudnick is thanked in particular for her patience and great editorial effort.

References

Abbott, D., Mooney, W., 1995. The structural and geochemical evolution of the continental crust support for the oceanic plateau model of continental growth. Rev. Geophys. Suppl. Uni. Geodesy Geophys. 1991–94, 231–242.

Abbott, D.H., Drury, R., Mooney, W.D., 1997. Continents as lithological icebergs: the importance of buoyant lithospheric roots. Earth Planet. Sci. Lett. 149, 15–27.

Albarède, F., 1998. The growth of continental crust. Tectonophysics 296, 1–14.

Allègre, C.J., 34 others, 1984. Structure and evolution of the Himalayan–Tibet orogenic belt. Nature 307, 17–22.

Arculus, R.J., 1981. Island arc magmatism in relation to the evolution of the crust and mantle. Tectonophysics 75, 113–133.

Barth, M., McDonough, W.F., Rudnick, R.L., 2000. Tracking the budget of Nb and Ta in the continental crust. Chem. Geol 165, 197–213.
Bowen, N.L., 1928. The Evolution of the Igneous Rocks. Princeton University Press, Princeton, NJ. (332 pp.).
Brenan, J.M., Shaw, H.F., Ryerson, F.J., Phinney, D.L., 1995. Experimental-determination of trace-element partitioning between pargasite and a synthetic hydrous andesitic melt. Earth Planet. Sci. Lett 135, 1–11.
Castillo, P.R., 2006. An overview of adakite petrogenesis. Chinese Sci. Bull 51, 257–268.
Chu, M.F., Chung, S.L., Song, B., Liu, D., O'Reilly, S.Y., Pearson, N.J., 2006. Zircon U–Pb and Hf isotope constrains on the Mesozoic tectonics and crustal evolution of southern Tibet. Geology 34, 745–748.
Clift, P., Vannucchi, P., 2004. Controls on tectonic accretion versus erosion in subduction zones: implications for the origin and recycling of the continental crust. Rev. Geophys. 42, RG2001. doi:10.1029/2003RG000127 (31 pp.).
Condie, K.C., 2000. Episodic continental growth models: afterthoughts and extensions. Tectonophysics 322, 153–162.
Copeland, P., Harrison, T.M., Kidd, W.S.F., Xu, R., Zhang, Y., 1987. Rapid early Miocene acceleration of uplift in the Gangdese Belt, Xixang (southern Tibet), and its bearing on the accommodation mechanisms of the India–Asia collision. Earth Planet. Sci. Lett. 86, 240–252.
Coulon, C., Maluski, H., Bollinger, C., Wang, S., 1986. Mesozoic and Cenozoic volcanic rocks from central and southern Tibet: $^{39}Ar/^{40}Ar$ dating, petrological characteristics and geodynamical significance. Earth Planet. Sci. Lett 79, 281–302.
Davidson, J.P., Arculus, R.J., 2006. The significance of Phanerozoic arc magmatism in generating continental crust. In: Brown, M., Rushmer, T. (Eds.), Evolution and Differentiation of the Continental Crust. Cambridge Press, pp. 135–172.
Defant, M.J., Drummond, M.S., 1990. Derivation of some modern arc magmas by melting of young subducted lithosphere. Nature 347, 662–665 (1990).
Dewey, J.F., Shackelton, R.M., Chang, C., Sun, Y., 1988. The tectonic evolution of the Tibetan Plateau. Phil. Trans. R. Soc. Lond. A327, 379–413.
Dong, G., 2002. Linzizong Volcanic Rocks and Implications for Probing India-Eurasia Collision Process in Linzhou Volcanic Basin, Tibet, China University of Geosciences, PhD Thesis (in Chinese), 150 pp.
Dong, G., Mo, X., Zhao, Z., Guo, T., Wang, L., Chen, T., 2005. Geochronologic constraints on the magmatic underplating of the Gangdese Belt in the India–Eurasia collision: evidence of SHRIMP II zircon U–Pb dating. Acta Geol. Sin. 79, 787–794.
Elliott, T., 2003. Tracers of the slab. Geophys. Monogr 238, 23–45.
England, P., 1993. Convective removal of thermal boundary layer of thickened continental lithosphere; a brief summary of causes and consequences with special reference to the Cenozoic tectonics of the Tibetan Plateau and surrounding regions. Tectonophysics 223, 67–73.
England, P., Houseman, G., 1989. Extension during continental convergence, with application to the Tibetan Plateau. J. Geophys. Res 94, 17561–17579.
Fan, W.M., Guo, F., Wang, Y.J., Ge, L., 2003. Late Mesozoic calcalkaline volcanism of post-orogenic extension in the northern Da Hinggan Mountains, northeastern China. J. Volcanol. Geotherm. Res. 121, 115–135.
Flower, M., Russo, R.M., Tamaki, K., Nguyen, H., 2001. Mantle contamination and the Izu–Bonin–Mariana (IBM) 'high-tide mark': evidence for mantle extrusion caused by Tethyan closure. Tectonophysics 333, 9–34.
Foley, S., Barth, M.G., Jenner, G.A., 2000. Rutile/melt partition coefficients for trace elements and an assessment of the influence of rutile on the trace element characteristics of subduction-zone magmas. Geochim. Cosmochim. Acta 64, 933–938.
Foley, S., Tiepolo, M., Vannucci, R., 2002. Growth of early continental crust controlled by melting of amphibolite in subduction zones. Nature 417, 837–840.
Gao, S., Zhang, B.R., Jin, Z.M., Kern, H., Luo, T.C., Zhao, Z.D., 1998. How mafic is the lower continental crust? Earth Planet. Sci. Lett. 106, 101–117.
Gill, J.B., 1981. Orogenic Andesites and Plate Tectonics. Springer-Verlag, New York. (390 pp.).
Green, T.H., Pearson, N.J., 1987. An experimental study of Nb and Ta partitioning between Ti-rich minerals and silicate liquids at high pressure and temperature. Geochim. Cosmochim. Acta 51, 55–62.
Guo, T., Liang, D., Zhang, Y., et al., 1991. Geology of Ngari, Tibet (Xizang). The China University of Geosciences Press, Wuhan. (in Chinese).
Guo, Z., Wilsom, M., Liu, J., 2007. "Post-collisional adakites in South Tibet" products of partial melting of subduction-modified lower crust. Lithos 96, 205–224.
Harris, N.B.W., Pearce, J.A., Tindle, A.G., 1986. Geochemical characteristics of collisional-zone magmatism. In: Coward, M.P., Reis, A.C. (Eds.), Collision tectonics. Geol. Soc. Spec. Publ., 19, pp. 67–81.
Hawkesworth, C.J., Kemp, A.I.S., 2006. The differentiation and rates of generation of the continental crust. Chem. Geol 226, 134–143.
Hirose, K., 1997. Melting experiments on lherzolite KLB-1 under hydrous conditions and generation of high-magnesian andesitic melts. Geology 25, 42–44.
Hou, Z.Q., Gao, Y.F., Qu, X.M., Rui, Z.Y., Mo, X.X., 2004. Origin of adakitic intrusives generated during mid-Miocene east–west extension in South Tibet. Earth Planet. Sci. Lett. 220, 139–155.
Jahn, B.M., Griffin, W.L., Windley, B.F., 2000a. Continental growth in the Phanerozoic: evidence from Central Asia Special issue. Tectonophysics 328, 1–227.
Jahn, B.M., Wu, F.Y., Chen, B., 2000b. Massive granitoids generation in Central Asia: Nd isotope evidence and implication for continental growth in the Phanerozoic. Episodes 23, 82–92.
Jiang, W., Mo, X., Zhao, C., Guo, T., Zhang, S., 1999. Geochemical characteristics of granitoids and mafic microgranular enclaves in middle Gangdese of Tibetan Plateau. Acta Petrol. Sinica 15, 89–97.
Jin, C., Zhou, Y., 1978. Magmatic rocks in the Himalayan Gangdese. Geol. Sci. 4, 297–311 (in Chinese).
Jin, C., Xu, R., 1982. Granitoids in Himalayas and middle Gangdese. Petrol. Res. 1, 81–95 (in Chinese with English abstract).
Johnson, M.C., Plank, T., 1999. Dehydration and melting experiments constrain the fate of subducted sediments. Geochem. Geophys. Geosyst. 1 (29 pp.).
Jull, M., Kelemen, P.B., 2001. On the conditions for lower crustal convective stability. J. Geophys. Res 106, 6423–6446.
Kapp, P., Murphy, M.A., Yin, A., Harrison, T.M., Ding, L., Guo, J., 2003. Mesozoic and Cenozoic tectonic evolution of the Shiquanhe area of western Tibet. Tectonics 22, 1029. doi:10.1029/2001TC001332.
Kapp, P., Yin, A., Harrison, T.M., Ding, L., 2005. Cretaceous–Tertiary shortening, basin development, and volcanism in central Tibet. Geol. Soc. Amer. Bull 117, 865–878.
Kapp, P., DeCelles, P.G., Leier, A.L., Fabijanic, J.M., He, S., Pullen, A., Gehrels, G.E., 2007. The Gangdese resroarc thrust belt revealed. GSA Today 17, 4–9.
Kay, R.W., Kay, S.M., 1993. Delamination and delamination magmatism. Tectonophysics 219, 177–189.
Kelemen, P.B., 1995. Genesis of high Mg andesites and the continental crust. Contrib. Mineral. Petrol 120, 1–19.
Kelemen, P.B., Hanghoj, K., Greene, A.R., 2003a. One view of the geochemistry of subduction-related magmatic arcs with an emphasis on primitive andesite and lower crust. Treatise on Geochemistry, vol. 3, pp. 593–660.
Kelemen, P.B., Yogodzinski, G.M., Scholl, D.W., 2003b. Along-strike variation in lavas of Aleutian island arcs: genesis of high Mg# andesite and implications for continental crust, in inside the subduction factory. Geophys. Monogr. 238, 223–276.
Kelemen, P.B., Rilling, J.L., Parmentier, E.M., Mehl, L., Hacker, B.R., 2003c. Thermal structure due to solid-state flow in the mantle wedge beneath arcs. Geophys. Monogr 238, 293–311.
Kemp, A.I.S., Hawkesworth, C.J., Paterson, B.A., Kinny, P.D., 2006. Episodic growth of the Gondwana supercontinent from hafnium and oxygen isotopes in zircon. Nature 439, 580–583.
Kerr, A.C., 2003. Oceanic plateaus. Treatise on Geochemistry, vol. 3, pp. 537–566.
Kramers, J.D., Tolstikhin, I.N., 1997. Two terrestrial lead isotope paradoxes, forward transport modelling, core formation and the history of the continental crust. Chem. Geol 139, 75–110.
Kushiro, I., Syono, Y., Akimoto, S., 1968. Melting of a peridotite nodule at high pressures and high water pressures. J. Geophys. Res. 73, 6023–6029.
La Bas, M.J., Le Maitre, R.W., Streckeisen, A., Zanettin, B., 1986. A chemical classification of volcanic rocks based on the total alkali–silica diagram. J. Petrol 27, 745–750.

Leeder, M.R., Smith, A.B., Jixiang, Y., 1988. Sedimentology and palaeoenvironmental evolution of the 1985 Lhasa to Golmud Geotraverse. Phil. Trans. R. Soc. Lond. A327, 107–143.

Le Fort, P., 1988. Granites in the tectonic evolution of Himalaya. Phil. Trans. R. Soc. Lond 326, 281–299.

Mahoney, J.J., Frei, R., Tejada, M.L.G., Mo, X.X., Leat, P.T., 1998. Tracing the Indian ocean mantle domain through time: isotopic results from old west Indian, east Tethyan and south Pacific seafloor. J. Petrol 39, 1285–1306.

Maluski, H., Proust, F., Xiao, X.C., 1982. $^{39}Ar/^{40}Ar$ dating of the TransHimalyan calc-alkaline magmatism of southern Tibet. Nature 298, 152–156.

McCulloch, M.T., Bennett, V.C., 1994. Progressive growth of the Earth's continental crust and depleted mantle: geochemical constraints. Geochim. Cosmochim. Acta 58, 4717–4738.

McDonough, W.F., Sun, S.S., 1995. The composition of the Earth. Chem. Geol. 120, 223–253 (1995).

Mez-Tuena, A., Langmuir, C.H., Goldstein, S.L., Straub, S.M., Ortega-Gutierrrez, F., 2007. Geochemical evidence for slab melting in the trans-Mexican volcanic belt. J. Petrol. 48, 537–562.

Mo, X., Zhao, Z., Deng, J., Dong, G., Zhou, S., Guo, T., Zhang, S., Wang, L., 2003. Response of volcanism to the India–Asia collision. Earth Sci. Front 10, 135–148.

Mo, X., Dong, G., Zhao, Z., Guo, T., Wang, L., Chen, T., 2005. Timing m mixing in the Gangdese magmatic belt during the India–Asia collision: zircon SHRIMP U–Pb dating. Acta Geol. Sinica 79, 66–76.

Mo, X., Zhao, Z., Deng, J., Flower, M., Yu, X., Luo, Z., Li, Y., Zhou, S., Dong, G., Zhu, D., Wang, L., 2006. Petrology and geochemistry of postcollisional volcanic rocks from the Tibetan plateau: implications for lithosphere heterogeneity and collision-induced asthenospheric mantle flow. In: Dilek, Y., Pavlides, S. (Eds.), Postcollisional tectonics and magmatism in the Mediterranean region and Asia. Geol. Soc. Am. Spec. Pap., vol. 409, pp. 507–530.

Mo, X., Hou, Z., Niu, Y., Dong, G., Qu, X., Zhao, Z., Yang, Z., 2007. Mantle contributions to crustal thickening in south Tibet in response to the India–Asia collision. Lithos 96, 225–242.

Mo, X., Zhao, Z., Zhou, S., Dong, G., Guo, T., Liang, W., 2002. Evidence for timing of the initiation of India–Asia collision from igneous rocks in Tibet. EOS Trans. AGU 83 (47), S62B–S1201 (Fall Meet. Suppl.).

Murphy, M.A., Yin, A., Harrison, T.M., Durr, S.B., Chen, Z., 1997. Significant crustal shortening in south-central Tibet prior to the Indo-Asian collision. Geology 25, 719–722.

Nichols, G.T., Wyllie, P.J., Stern, C.R., 1994. Subduction zone melting of pelagic sediments constrained by melting experiments. Nature 371, 785–788.

Niu, Y., 2005. Generation and evolution of basaltic magmas: Some basic concepts and a hypothesis for the origin of the Mesozoic–Cenozoic volcanism in eastern China. Geol. J. China Univ. 11, 9–46.

Niu, Y., Lesher, C.M., 1991. Hydrothermal alteration of mafic metavolcanic rocks and genesis of Fe–Zn–Cu sulfide deposits, Stone Hill district, Alabama. Econ. Geol. 86, 983–1001.

Niu, Y., Waggoner, G., Sinton, J.M., Mahoney, J.J., 1996. Mantle source heterogeneity and melting processes beneath seafloor spreading centers: the East Pacific rise 18°–19°S. J. Geophys. Res. 101, 27711–27733.

Niu, Y., Batiza, R., 1997. Trace element evidence from seamounts for recycled oceanic crust in the eastern equatorial Pacific mantle. Earth Planet. Sci. Lett. 148, 471–484.

Niu, Y., Collerson, K.D., Batiza, R., Wendt, J.I., Regelous, J.I., 1999. The origin of E-Type MORB at ridges far from mantle plumes: the East Pacific rise at 11°20'N. J. Geophys. Res. 104, 7067–7087.

Niu, Y., Bideau, D., Hékinian, R., Batiza, R., 2001. Mantle compositional control on the extent of melting, crust production, gravity anomaly and ridge morphology: a case study at the Mid-Atlantic Ridge 33–35°N. Earth Planet. Sci. Lett. 186, 383–399.

Niu, Y., Regelous, M., Wendt, J.I., Batiza, R., O'Hara, M.J., 2002a. Geochemistry of near-EPR seamounts: importance of source vs. process and the origin of enriched mantle component. Earth Planet. Sci. Lett. 199, 327–345.

Niu, Y., Gilmore, T., Mackie, S., Greig, A., Bach, W., 2002b. Mineral chemistry, whole-rock compositions and petrogenesis of ODP Leg 176 gabbros: data and discussion. In: Natland, J.H., Dick, H.J.B., Miller, D.J., Von Herzen, R. P. (Eds.), Proc. Ocean Drill. Prog., vol. 176, pp. 1–60.

Niu, Y., O'Hara, M.J., 2003. The origin of ocean island basalts (OIB): a new perspective from petrology, geochemistry and mineral physics considerations. J. Geophys. Res. 108. doi:10.1029/2002JB002048 (19 pp.).

Niu, Y., O'Hara, M.J., Pearce, J.A., 2003. Initiation of subduction zones as a consequence of lateral compositional buoyancy contrast within the lithosphere: a petrologic perspective, J. Petrol. 44, 851–866.

O'Hara, M.J., 1965. Primary magmas and the origin of basalts. Scott. J. Geol. 1, 19–40.

Othman, D.B., Polve, M., Allegre, C.J., 1984. Nd–Sr isotopic composition of granulites and constraint on the evolution of the lower continental crust. Nature 307, 510–515.

Pan, G.T., Ding, J., Yao, D.S., 2004. Geological Map of Qinghai–Xizang (Tibet) Plateau and Adjacent Areas (with a Guidebook) (1:2500,000), Chengdu, Chengdu Cartographic Publishing House.

Peacock, S.M., 2003. Thermal structure and metamorphic evolution of subducting slabs, in inside the subduction factory. Geophys. Monogr. 238, 7–22.

Peacock, S.M., Wang, K., 1999. Seismic consequences of warm versus cool subduction zone metamorphism: examples from northeast and southeast Japan. Science 286, 937–939.

Pearce, J.A., Mei, H., 1988. Volcanic rocks of the 1985 Tibet Geotraverse Lhasa to Golmud. Phil. Trans. R. Soc. Lond. A327, 203–213.

Pearcy, J.G., DeBari, S.M., Slep, N.H., 1990. Mass balance calculations for two sections of island arc crust and implications for the formation of continents. Earth Planet. Sci. Letts. 96, 427–442.

Plank, T., 2005. Constraints from Thorium/Lanthanum on sediment recycling at subduction zones and the evolution of continents. J. Petrol. 46, 921–944.

Plank, T., Langmuir, C.H., 1998. The chemical compositions of subducting sediments and its consequences for the crust and mantle. Chem. Geol. 145, 325–394.

Polat, A., Kerrich, R., Wyman, D.A., 1998. The late Archean Schreiber–Hemlo and White River-Dayohessarah greenstone belts, Superior Province: Collages of oceanic plateaus, ocean arcs, and subduction-accretion complexes. Tectonophysics 289, 295–326.

Reymer, A., Schubert, G., 1984. Phanerozoic addition rates to the continental crust and crustal growth. Tectonics 3, 63–77.

Rickwood, P.C., 1989. Boundary lines within petrologic diagrams which use oxides of major and minor elements. Lithos 55, 121–137.

Rudnick, R.L., 1995. Making continental crust. Nature 378, 571–578.

Rudnick, R.L., Fountain, D.M., 1995. Nature and composition of the continental crust: a lower crustal perspective. Rev. Geophys. 33, 267–309.

Rudnick, R.L., Gao, S., 2003. Composition of the continental crust. Treatise on Geochemistry, vol. 3, pp. 1–64.

Rudnick, R.L., Gao, S., Ling, W.L., Liu, Y.S., McDonough, W.F., 2004. Petrology and geochemistry of spinel peridotite xenoliths from Hannuoba and Qixia, North China craton. Lithos 77, 609–637.

Scharer, U., Xu, R., Allegre, C.J., 1984. U–Pb geochronology of Gangdese (Transhimalaya) plutonism in the Lhasa–Xigaxe region, Tibet. Earth Planet. Sci. Lett. 69, 311–320.

Scholl, D.W., von Huene, R., 2004. Recycling of continental crust at ocean margin subduction zones: evidence and implications for the growth of continental crust and supercontinent reconstruction. Presentation at "Plate Tectonic, Plumes and Planetary Lithospheres Conference — Celebration of Kevin Burke's 75th Birthday", Houston, November 12-15, 2004.

Staudigel, H., 2003. Hydrothermal alteration processes in the oceanic crust. Treatise on Geochemistry, vol. 3, pp. 511–535.

Stein, M., Hofmann, A.W., 1994. Mantle plumes and episodic crustal growth. Nature 372, 63–68.

Stern, C.R., Huang, W.L., Wyllie, P.J., 1975. Basalt–andesite–rhyolite–H_2O: crystallization intervals with excess H_2O and H_2O — undersaturated liquidus surfaces to 35 kbar, with implications for magma genesis. Earth Planet. Sci. Lett. 28, 189–196.

Sun, S.s., McDonough, W.F., 1989. Chemical and isotopic systematics of ocean basalt: implications for mantle composition and processes. In: Saunders, A.

D., Norry, M.J. (Eds.), Magmatism of the Ocean Basins. Geol. Soc. Spec. Publ., vol. 42, pp. 323–345.

Takahashi, N., Kodaira, S., Klemperer, L.S., et al., 2007. Crustal structure and evolution of the Mariana intra-oceanic island arc. Geology 35, 203–206.

Tatsumi, Y., 2006. High-Mg Andesites in the Setouchi volcanic belt, Southwestern Japan: analogy to archean magmatism and continental crust formation? Annual Rev. Earth Planet Sci. 34, 467–499.

Taylor, S.R., 1967. The origin and growth of continents. Tectonophysics 4, 17–34.

Taylor, S.R., 1977. Island arc models and the composition of the continental crust. In: Talwani, M., PitmanIII III, W.C. (Eds.), Island Arcs, Deep Sea Trenches, and Back-Arc Basins. . Maurice Ewing Ser., vol. 1. AGU, Washington, D.C., pp. 325–335.

Taylor, S.R., McLennan, S.M., 1985. The continental crust: Its composition and evolution. Blackwell, Oxford. (312 pp.).

Taylor, S.R., McLennan, S.M., 1995. The geochemical evolution of the continental crust. Rev. Geophys. 33, 241–265.

Tiepolo, M., Vannucci, R., Oberti, R., Foley, S., Bottazzi, P., Zanetti, A., 2000. Nb and Ta incorporation and fractionation in titanian pargasite and kaersutite: crystal-chemical constraints and implications for natural systems. Earth Planet. Sci. Lett. 176, 185–201.

Vielzeuf, D., Schmidt, M.W., 2001. Melting relations in hydrous systems revisited: application to metapelites, metagreywackes and metabasalts. Contrib. Mineral. Petrol. 141, 251–267.

von Huene, Scholl, D.W., 1991. Observations at convergent margins concerning sediment subduction, subduction erosion, and the growth of continental crust. Rev. Geophys. 29, 279–316.

Wedepohl, H., 1995. The composition of the continental crust. Geochim. Cosmochim. Acta 59, 1217–1239.

Willems, H., Zhou, Z., Zhang, B., Grafe, K.U., 1996. Stratigraphy of the Upper Cretaceous and Lower Tertiary strata in the Tethyan Himalayas of Tibet (Tingri area, China). Geol. Rundsch. 85, 723–754.

Wolf, M.B., Wyllie, P.J., 1994. Dehydration melting of amphibolite at 10 kbar: effects of temperature and time, Contrib. Mineral. Petrol. 115, 369–383.

Wyllie, P.J., 1979. Magmas and volatile components. Am. Mineral. 64, 469–500.

Wyllie, P.J., Wolfe, M.B., 1993. Dehydration-melting of amphibolite: sorting out the solidus. In: Prichard, H.M., Alabaster, T., Harris, N.B.W., Near, C.R. (Eds.), Magmatic Processes and plate tectnics. Geol. Soc. Spec. Publ., vol. 76, pp. 405–416.

Xu, R.H., Schärer, U., Allègre, C.J., 1985. Magmatism and metamorphism in the Lhasa block (Tibet): a geochronological study. J. Geol 93, 41–57.

Yin, A., Harrison, T.M., 2000. Geologic evolution of the Himalayan Tibetan Orogen. Ann. Rev. Earth Planet. Sci. 28, 211–280.

Yin, J., Xu, J., Liu, C., Li, H., 1988. The Tibetan plateau: regional stratigraphic context and previous work. Phil. Trans. R. Soc. Lond. A327, 5–52.

Yin, A., Harrison, T.M., Murphy, M.A., Grove, M., Nie, S., 1999. Tertiary deformation history of southeastern and southwestern Tibet during the Indo-Asian collision. Geol. Soc. Am. Bull. 111, 1644–1664.

Yue, Y., Ding, L., 2006. $^{40}Ar/^{39}Ar$ geochronology, geochemical characteristics and genesis of the Linzhou basin dikes, Tibet. Acta Petrol. Sin. 22, 855–866.

Zhang, H.F., Sun, M., Zhou, X.H., Fan, W.M., Zhai, M.G., Yin, J.F., 2002. Mesozoic lithosphere destruction beneath the North China Craton: evidence from major-, trace-element and Sr–Nd–Pb isotope studies of Fangcheng basalts. Contrib. Mineral. Petrol. 144, 241–253.

Zhang, S.Q., Mahoney, J.J., Mo, X.X., Ghazi, A.M., Milani, L., Crawford, A.J., Guo, T.Y., Zhao, Z.D., 2005. Evidence for a widespread Tethyan upper mantle with Indian-ocean-type isotopic characteristics. J. Petrol. 46, 829–858.

Zhou, S., Mo, X., Dong, G., Zhao, Z., Qiu, R., Guo, T., Wang, L., 2004. $^{40}Ar–^{39}Ar$ geochronology of Cenozoic Linzizong volcanic rocks from Linzhou Basin, Tibet, China and their geological implications. Chinese Sci. Bull. 49, 1970–1979.